AN ABSTRACT OF THE THESIS OF

Bosong Li for the degree of Master of Science in Materials Science presented on November 30, 2015.

Title: Effect of Imprinting Process on Fracture Behavior of a Zr-based Bulk Metallic Glass

Abstract approved: ____

Jamie J. Kruzic

Bulk metallic glasses (BMGs) are relatively new amorphous materials that have received much attention in recent years. Rapid cooling methods from the liquid state provides the possibility to bypass crystallization during solidification. Due to the lack of crystal defects such as grain boundaries and dislocations, BMGs can have some special properties such as high yield strength and high elastic strain limit. Fracture toughness is also an important mechanical property for engineering design. Understanding the fracture behavior of BMGs is necessary for mechanical applications and material specifications.

In recent year studies, it has been shown that the fracture toughness of different BMGs varies significantly from brittle to quite high damage tolerance. However, BMGs have been reported to have large variability in mode I fracture toughness even for a single composition. The primary aim of this thesis project is to understand the effect of one thermomechanical method on the fracture behavior of BMGs. In this study, alternating soft and hard regions were created in a $Zr_{52.5}Ti_5Cu_{18}Ni_{14.5}Al_{10}$ (at.%) BMG via mechanical imprinting at room temperature. The results showed that only 50% of as-cast samples demonstrated plastic deformation during mode I fracture tests while 100% of imprinted samples demonstrated measurable plasticity and the scatter in measured mode I fracture toughness was significantly reduced.

Besides the improved fracture reliability reflected from J-integral and K_J values, imprinted samples also showed more tortuous crack trajectory than as-cast samples. By studying the fracture surfaces, it was found that high toughness samples showed four distinct regions on the fracture surface originating from the end of fatigue pre-crack which are crack blunting region (I), Taylor meniscus instability region (II), stair-like steps region (III), and flat dimple pattern region (IV). However, the low toughness samples only show three regions with no evidence of region (III). It was found that dimple sizes in the fracture surfaces vary from 2 to 12μm by the line intercept method for low to high toughness samples, respectively. Finally, by correlating fracture toughness values (K_J) and dimple sizes (w), a linear association between K_J^2 and w was constructed. Overall, mechanical treatments show promise for improving fracture reliability of BMGs.

Effect of Imprinting Process on Fracture Behavior of a Zr-based Bulk Metallic Glass

by
Bosong Li

A THESIS

submitted to

Oregon State University

in partial fulfillment of
the requirements for the
degree of

Master of Science

Presented November 30, 2015
Commencement June 2016

Master of Science thesis of Bosong Li presented on November 30, 2015

APPROVED:

Major Professor, representing Materials Science

Director of the Materials Science Program

Dean of the Graduate School

I understand that my thesis will become part of the permanent collection of Oregon State University libraries. My signature below authorizes release of my thesis to any reader upon request.

Bosong Li, Author

ACKNOWLEDGEMENTS

The author expresses sincere appreciation to Dr. Jamie Kruzic for his continued guidance and advice as adviser through the research project, Hamed Shahabi for offering the BMG samples, Dr. Warnes, Dr. Tucker, Dr. Stuedlein for guidance as committee members, Teresa Sawyer for her training and help on SEM.

The author would also like to express personal appreciation to all group members and friends for their support and encouragement throughout my study.

TABLE OF CONTENTS

TABLE OF CONTENTS (Continued)

LIST OF FIGURES

LIST OF FIGURES (Continued)

LIST OF TABLES

1. Introduction

1.1 Metallic glasses

In contrast to conventional metallic materials that possess translational symmetry, metallic glass is defined as a non-crystalline amorphous solid in which atoms are randomly arranged without long-range order. Also different from most of the ‘window glasses’ that we encounter in life, glasses containing metallic components are not transparent and also display a local order based on icosahedral nano-structures [1]. To obtain metallic glasses, rapid cooling liquids directly to temperatures below the glass transition temperature, T_g, is one of the most common methods. This allows the glass to solidify while bypassing crystallization. Therefore, metallic glasses can be regarded as amorphous frozen liquids. While metallic glasses are always amorphous, not all amorphous materials are glass. Glass is any non-crystalline solid obtained by continuous cooling from liquid state, and amorphous solid is any non-crystalline material obtained by any other method, such as vapor deposition, mechanical alloying, high energy electron irradiation, etc. [2]. Bulk metallic glasses (BMGs) which have a thickness of at least a few millimeters typically possess some special characteristics:

- The alloy system always contain a minimum of three components;
- The required solidification rate is much slower, typically $<10^3$ K/s, than for ribbons and wires;
- They exhibit a large undercooled region which keeps BMGs rather ‘stable’ at ambient temperatures.

Even though some other techniques, like thermoplastic forming [3], are used for fabricating BMGs, the most common way to produce BMGs is the rapid quenching method using copper mold casting techniques. For BMGs produced by this method, the glass-forming ability is determined by the critical cooling rate which is the minimum cooling rate necessary to bypass crystallization. Therefore, reducing the critical cooling rate from a materials design perspective is essential for designing new BMGs. Due to the fact that glasses are not in a thermodynamic equilibrium state and have a higher intrinsic energy than crystalline alloys, BMGs are considered to be metastable. Alloys with lower critical cooling rates typically have a smaller energy difference between the amorphous and crystalline states, leading to a smaller driving force for crystallization [4]. Nowadays, critical cooling rate as low as 1K/s can be achieved to form BMGs [5].

1.2 History and development of metallic glasses

The first successful preparation of metallic glasses was brought about in 1960. By rapidly solidifying the liquids at a high rate, binary Au–Si alloys in the glassy state were obtained [6]. The amorphous nature of the quenched materials was confirmed by transmission electron microscopy using electron diffraction techniques in addition to X-ray diffraction. However, this amorphous alloy was quite unstable, and it crystallized in about three hours at room temperature. Because of the poor glass forming ability at that time, quite high cooling rates were always required which resulted in casting thickness of only a few micrometers. Since the first discovery of metallic glasses, much more efforts were made to explore new alloy systems and lower the critical cooling rate. The first publication of BMGs goes back to 1974, when Chen reported that by quenching ternary alloys of different compositions with a cooling rate less than 10^3K/s, he obtained metallic glasses with diameters of 1-3mm [7]. The development of BMGs with composition like Zr-Cu-Ni-Al and Zr-Ti-Ni-Cu-Be for practical uses started in the 1990s [8, 9]. At the same time, the discovery of new alloy compositions of La-, Mg-, and Pd-based BMGs stimulated much research activities [10-12]. The multiplication of these alloy compositions led to a significant increase in glass forming ability, and hence the production of glassy alloys with thickness or diameters of several millimeters, or even centimeters, could be achieved.

The endeavor of widespread commercialization into applications revealed a number of disadvantages when used as structural hardware, particularly the low fracture toughness, low fatigue limit and lack of ductility [13, 14]. Since then, research directed at toughening and increasing the plasticity of BMGs has been of interest. One of the effective ways involves introducing some inhomogeneity [15] into the glassy structure and the other one is developing composite materials with a bulk metallic glass matrix [16, 17].

1.3 Glass-forming ability of metallic glasses

Generally, the formation of metallic glasses requires a high cooling rate and sluggish crystallization kinetics. A simple way to visualize these concepts above can be realized from a time-temperature-transformation diagram, the so called TTT diagram. As can be seen from Fig. 1 [18], the TTT diagram of $Zr_{52.5}Cu_{17.9}Ni_{14.6}Al_{10}Ti_5$ BMG (Vitroley 105) display the glass forming ability information where temperature is plotted as a function of time to the onset of crystallization. As temperature decreases, the undercooling region becomes larger which results in a larger free energy difference (ΔG_{ls}) between liquid and solid phases. This free energy difference provides the increasing driving force for crystal nucleation. On the other hand, the growth rate of crystalline nuclei is diffusion controlled and decreases with lowering temperature. Therefore, the lowering temperature leads to a higher viscosity (η(T)) which hinders atomic arrangements in liquids. As a consequence, the formation of the typical "C-shape" arises from the competition between the increasing driving force for nucleation and the slowing down of crystallization kinetics. This can be seen from classical nucleation theory. The nucleation rate I_v is described in Eq. (1):

$$I_{\mathrm{v}} = \frac{A_{\mathrm{v}}}{\eta(\mathrm{T})} \exp\left(-\frac{16\pi\sigma^3 / \left(3\Delta G_{\mathrm{ls}}\right)^2}{k_{\mathrm{B}} T} \right) \tag{1}$$

where A_v is a constant and η (T) is the viscosity of the liquids; σ is the interfacial energy and ΔG_{ls} is the free energy difference between liquid and solid phases; k_B is the Boltzmann constant.

For conventional metals, when liquids are cooled from liquidus temperature T_l, the cooling rate is like curve two as indicated in Fig. 1. If the same liquid alloy is cooled from T_1 with faster solidification rate as indicated by curve one, then a glassy state could be achieved. That means if the temperature of the undercooled liquid is continuously decreased, the viscosity of the liquid will continue to increase, and the state of amorphous solid will be reached. Some critical cooling rate criteria for the glass formation have been presented by different authors [9, 19, 20], among which the most simple and accurate one is derived by Lin and Johnson [9]. As discussed above, the critical cooling rate required to avoid the formation of detectable crystallization in quenching liquid alloys can be used in describing the glass forming ability of materials. The critical cooling rate is related to the temperature gradient and cooling time as described in Eq. (2):

$$R_c = \frac{dT}{dt} = \frac{K(T_m - T_g)}{Cd^2} \tag{2}$$

where T_m and T_g are the initial melting temperature and glass transformation temperature respectively, d is the maximum attainable size, K is thermal conductivity and C is heat capacity per unit volume. By simplifying Eq. (2) based on values of typical molten alloys (T_m-T_g ~400 K, K~0.1 W/cm /K, C~4 J/cm^3/K), the maximum attainable size d (cm) in which a sample can be in fully amorphous structure can be determined by the critical cooling rate (R_c [K/s]) as in Eq. (3):

$$R_c = \frac{10}{d^2} \tag{3}$$

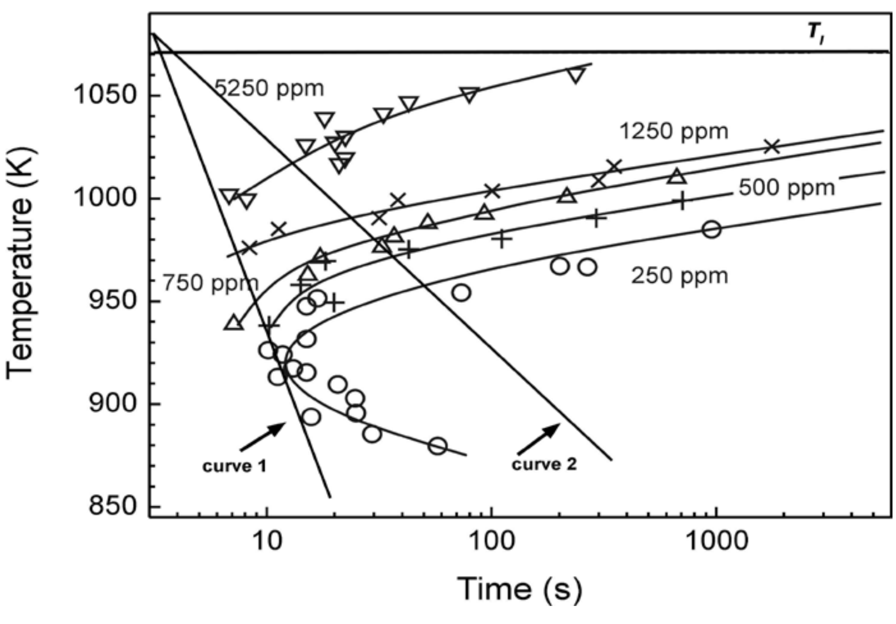

Figure 1. TTT diagram of Vitreloy 105 with 5250, 1250, 750, 500, 250 atom ppm oxygen (10000 ppm=1%). Reprinted with permission from [18].

Obviously, when the critical cooling rate is lowered, preparing samples with increasing thickness will be more easily realized. Table. 1 [21] presents the recent results of multicomponent BMGs with relative high critical dimensions produced by casting.

Base metal	Composition (at%)	critical dimensions(mm)	method
Pd	$Pd_{40}Ni_{40}P_{20}$ $Pd_{40}Cu_{30}Ni_{10}P_{20}$	10 72	Fluxing Water quenching
Zr	$Zr_{65}Al_{7.5}Ni_{10}Cu_{17.5}$ $Zr_{41.2}Ti_{13.8}Cu_{12.5}Ni_{10}Be_{22.5}$	16 25	Water quenching Copper mold casting
Cu	$Cu_{46}Zr_{42}Al_{7}Y_{5}$ $Cu_{49}Hf_{42}Al_{9}$	10 10	Copper mold casting Copper mold casting
Rare Earth	$Y_{36}Sc_{20}Al_{24}Co_{20}$ $La_{62}Al_{15.7}Cu_{11.15}Ni_{11.15}$	25 11	Water quenching Copper mold casting
Mg	$Mg_{54}Cu_{26.5}Ag_{8.5}Gd_{11}$ $Mg_{65}Cu_{7.5}Ni_{7.5}Zn_{5}Ag_{5}Y_{5}Gd_{5}$	25 14	Copper mold casting Copper mold casting
Fe	$Fe_{48}Cr_{15}Mo_{14}Er_{2}C_{15}B_{6}$ $Fe_{41}Co_{7}Cr_{15}Mo_{14}C_{15}B_{6}Y_{2}$	12 16	Copper mold casting Copper mold casting
Co	$Co_{48}Cr_{15}Mo_{14}C_{15}B_{6}Er_{2}$	10	Copper mold casting
Ti	$Ti_{40}Zr_{25}Cu_{12}Ni_{3}Be_{20}$	14	Copper mold casting
Ca	$Ca_{65}Mg_{15}Zn_{20}$	15	Copper mold casting
Pt	$Pt_{42.5}Cu_{27}Ni_{9.5}P_{21}$	20	Water quenching

Table 1. Summary of multicomponent BMGs with high critical dimensions. Data taken from [21].

To design BMG chemical compositions, however, the criteria are complex. Inoue [22] had concluded three basic rules for the fabrication of BMGs: (1) Three or more components must be contained within the alloy system. (2) A large difference (more than 12%) should exist between atomic sizes constituting the elements in the alloy. (3) Negative heats of mixing (exothermic) must exist among the main elements that leads to decreasing the atomic diffusivity and hence increasing the equilibrium melt viscosity.

1.4 Experimental techniques and microstructure of bulk metallic glasses

The microstructure of materials determine their macroscopic properties. However, due to the fact that metallic glasses lack translational and rotational symmetry found in crystals, it is challenging to determine atomic structure of bulk metallic glasses using conventional diffraction methodologies. Though some progress has been made in understanding the nature of short range order (SRO) of metallic glass [23, 24] the model of medium range order (MRO) is difficult to characterize and remains even less understood. The future development of a fundamental and comprehensive understanding of the microstructure and an accurate description of structural models is therefore essential for BMGs.

Experimental techniques have been extensively used to characterize micro-structure of metallic glasses. The amorphous nature of BMGs is initially investigated by X-ray diffraction (XRD) method. As is shown in Fig. 2 [25] the amorphous structure generally shows a broad diffuse peak without any detectable crystalline peaks in the XRD pattern. The peak is relatively weak compared with crystalline alloys. However, since the large temperature gradient during cooling can result in different structures between surface and inner material, synchrotron high energy X-ray diffraction is a more effective method in studying the amorphous nature and microstructure of BMGs. With synchrotron XRD (50-150 keV), high sample penetration can be reached that would reveal sharp diffraction spots originating from crystalline nanoparticles if it were to form during cooling. Besides that, it is also useful for analyzing medium range order cluster size [25].

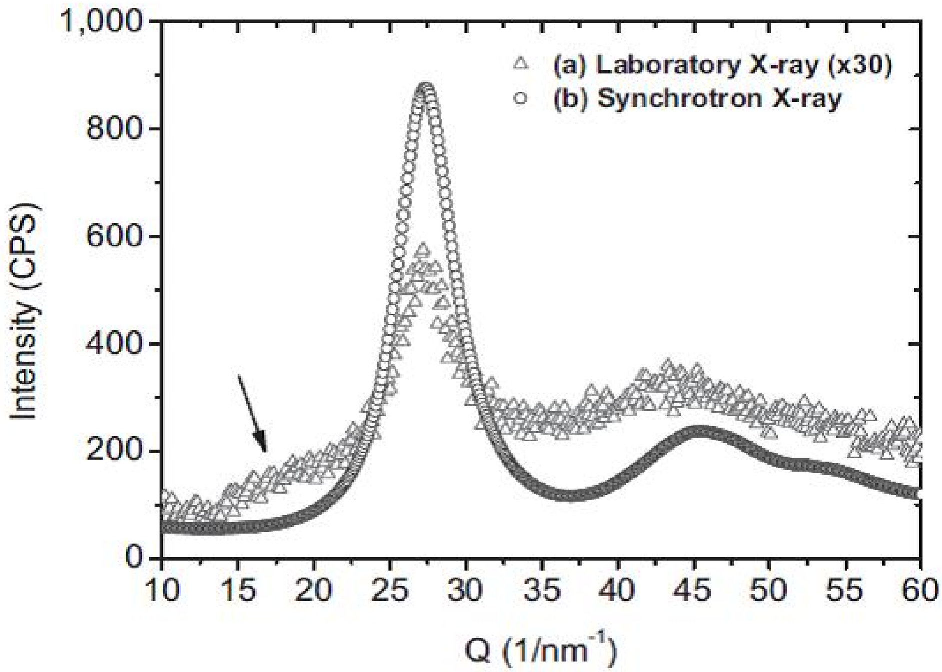

Figure 2. The X-ray diffraction pattern of the $Zr_{43}Cu_{43}Al_{7}Ag_{7}$ metallic glass using different X-ray sources: (a) The laboratory X-ray source intensity where the intensity was multiplied by 30 to provide a clear comparison with the data from the synchrotron experiment. (b) The synchrotron X-ray source. Reprinted with permission from [25].

As a useful technique, transmission electron microscopy (TEM) is widely used to characterize 3-D atomic-level structure in a projected 2-D image for crystals. In the case of BMGs, however, it is not useful for quantitative study of glassy structure due to no discernable structure in a projected image. Moreover, oxidation, crystallization, and even sample contamination can be induced during TEM sample preparation process. Therefore, although it is a reliable way to use TEM to confirm amorphous structure or test intrinsic heterogeneities, it is not a good choice for examining microstructure.

Fluctuation electron microscopy (FEM) can generate an electron probe beam in nano-scale which is on the same size scale needed for examining atomic structure on a length-scale of several nanometers. It has been shown effective for measuring the degree of ordering over medium range order in materials. But due to the fact that the variance peaks generated by FEM are more sensitive to the existence of nano-scale nuclei embedded in the glass matrix than to the variations of the cluster ordering in fully amorphous materials, using FEM to interpret MRO in BMGs is not straightforward [26].

Besides some restrictions in using traditional electron techniques to characterize the microstructure of BMGs, the lack of long range order also limits the direct analysis of structure models. A dense cluster-packing model of BMGs was proposed by Miracle in 2004 [23], who suggested that the efficiently packed cluster is composed by three topologically distinct solutes with solvent atoms in the first coordination shell. This structural model used crystallographic terminology to describe atomic structure and packing over a medium range of length scale and provides a good prediction of atomic concentrations. In this model, however, no orientational order was taken into account amongst the cluster which is different from the icosahedral model that will be discussed below.

In 1952, Frank first reported that icosahedron is the most desirable local order in monatomic metallic liquids [27]. After much study, icosahedral order became the most accepted description of atomic structures of metallic glass [28-31]. Recently, Hirata, et al. [1] reported experimental observations of local icosahedral order in a Zr-Pt metallic glass by means of angstrom-beam electron diffraction of single icosahedra. Also in Hirata's study, they found the icosahedra is distorted with partially face-centered cubic symmetry. These two observations together provide the evidence of geometric frustration of icosahedral structure of metallic glasses.

Besides the microstructure model, subatomic voids also exist as a result of short-to-medium range order. Tetrahedral and octahedral interstitial sites are considered voids in crystals. In BMGs, the distribution of voids might depend on the atomic packing of the system and can reveal important properties associated with structural defects. In other words, every atom is surrounded by other atoms in a coordination polyhedron. These local environments vary to some extent, and the space remaining between them is the excess volume (or free volume). Despite some possible limitations, free volume is frequently used as a simple and convenient indicator of the internal glass state.

Ding et al. [32] recently reported a statistical correlation between soft spots and shear transformation zones by molecular dynamics simulations employing the embedded atom method (EAM). The shear transformation zones are resulted from localized shear events and are considered as cooperative shearing of close-packed atomic clusters. Analogous to a 2D shear model glass, low-frequency vibrational modes were associated with soft spots where atoms tend to aggregate together with a length-scale of ~1nm. Upon loading, shear transformations easily initiating in soft spots was observed. Therefore, it is reasonable to conclude that heterogeneity is an inherent property in the amorphous structure that affects the spatial heterogeneity in the mechanical properties.

Beyond this discovery of atomic structure, the nanoscale microstructure analysis of metallic glasses is also necessary in describing macroscopic properties. To study the nanoscale microstructure of BMGs, Liu et.al [33] synthesized three different ZrCuNiAl BMGs through appropriate choices of composition. All materials in their experiment show significant improved compressive plasticity compared with their baseline ZrCuNiAl composition. TEM investigations revealed the microstructure of the more ductile BMGs is composed of isolated dark zones which extend from 2μm to 5μm and continuous bright zones which are in the range of 0.5μm to 1μm in width. This preferential thinning in bright zones indicates there are more unstable atomic volumes here, which result in that bright zones are softer than dark zones. Therefore, based on the fact that the hard regions surrounded by soft regions in the nanoscale microstructure gives improved ductility for metallic glasses, the possibility exists to achieve high plasticity using heterogeneous microstructures.

1.5 Mechanical properties of bulk metallic glasses

1.5.1 Comparisons with conventional materials

The lack of long-range order, grain boundaries and crystal defects in metallic glasses provides them with mechanical properties and behavior that are fundamentally different from that of crystalline materials. Fig. 3 [34] clearly shows a trend of elastic limit with Young's modulus of different material families. The contours of elastic strain σ_y/E indicates that most BMGs have a much higher value than other conventional metallic materials. Typically, bulk metallic glasses can exhibit attractive combinations of high yield strength (up to 2 GPa for Zr-based), high elastic strain limit (up to 2% for Zr-based) and relatively high fracture toughness. As presented in Fig. 4, the fracture toughness values of metals are high, while the low fracture toughness values suggest brittle nature of ceramics and glasses. In contrast, fracture toughness values vary over three to four orders of magnitude in the selected BMGs which range from about 2 MPa √ m, which is close to ceramics, to >100 MPa √ m, which is approaching the toughest metals.

Another mechanical property that should also be a concern for BMGs is the fatigue behavior, which is found to be in a wide range as a result of intrinsic and extrinsic factors [35-37]. Both crack initiation and crack propagation mainly contribute to the fatigue life of a component under cyclic loading. For conventional crystalline metals, the crack initiation stage constitutes large amounts of total fatigue life. However, initiation time in BMGs appears to be quite short, and thus, the main dominant factor affects fatigue life is crack growth stage. The threshold for fatigue-crack growth (ΔK_{TH}) in BMGs is usually ~ 2-3 MPa √ m [13]. Though comparable to that of aluminum alloys, the values lie at the low end of the range for crystalline metals. What's more, the endurance limit is also a main problem that needs considering for BMGs. Though BMGs with composition $Zr_{52.5}Cu_{17.9}Ni_{14.6}Al_{10}Ti_5$ have been reported with high fatigue endurance limit and a 10^7-cycle fatigue ratio, which is the ratio of fatigue strength to ultimate tensile strength, of ~0.24 [38, 39] that is even comparable to many metallic alloys, some others with fatigue ratio as low as 0.04 [40] have also been observed.

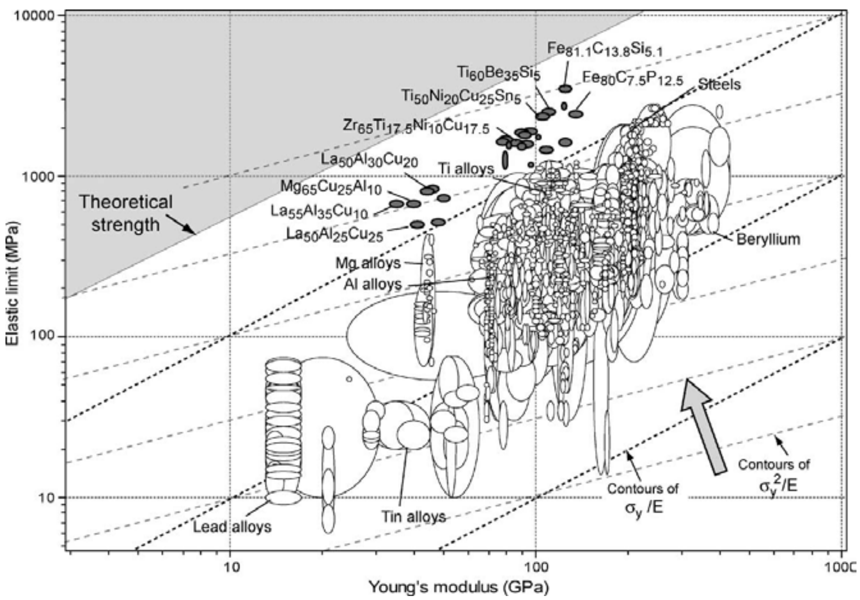

Figure 3. Materials selection map of yield strength vs. Young's modulus for comparisons between some BMGs and conventional materials. Reprinted with permission from [34].

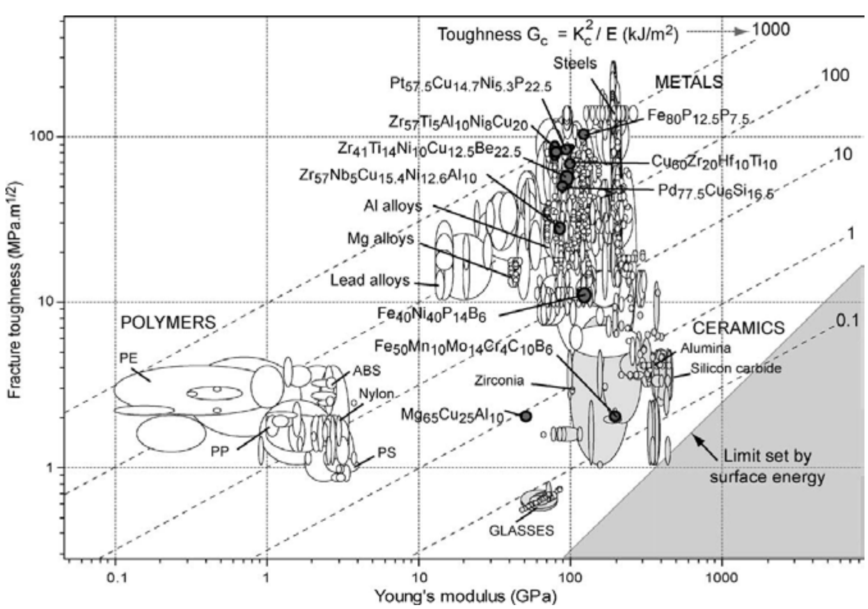

Figure 4. Materials selection map of fracture toughness vs. Young's modulus for comparisons between some selections of BMGs and conventional materials. Reprinted with permission from [34].

1.5.2 Mechanism of deformation

Unlike crystalline metals in which the main characteristic process dominating plastic deformation is dislocation glide, in BMGs shear transformation zones (STZs) are considered as the basic shear unit for plastic flow. The STZ theory was first suggested by Argon [41] who showed the local cooperative rearrangement of atoms can be well explained by the bubble rafts. It should be noted that unlike dislocations, which are structural defects in metals, STZs are defined by their transience: an observer cannot observe an STZ in the structure in an instant of time, and it is only a change in microstructure from one moment to the next [42]. In other words, STZs are events occurring in the local volume but not a feature of metallic glass structure. Schuh and Lund [43] further added that the percolation of shear transformation zones (STZs) promotes the formation and propagation of shear bands.

Spaepen [44] first proposed the concept of free volume that can be regarded as a structural parameter and governs the viscosity in the shear bands. The lowering of viscosity inside shear bands, therefore, must be accompanied by an increase of free volume. The accumulation of free volume created can result in local softening. Due to local softening, the region within the shear band deforms more easily than the rest of the material [45]. After a few shear bands are activated, severe plastic flow localization occurs and immediate catastrophic failure often happens.

As mentioned in section 1.4, since whether a region is prone to a shear transformation or not depends on the local microstructure [46], the shear transformation would preferentially occur in soft regions in BMGs and evolve into shear bands upon loading. When profuse shear bands are activated in soft regions, it is expected that localized plastic strain would distribute more uniformly and it would be less likely that one detrimental single shear band would form and propagate. Using this strategy to analyze the microstructure can present useful guidelines for designing BMGs with improved plasticity that will be discussed in section 2.

1.5.3 Plastic deformation and shear bands sliding behavior

Plastic deformation mechanism of BMGs as discussed above can be regarded as the accumulation of local strains induced by the movement of STZs and the redistribution of free volume. Depending on the temperature and strain rate, plastic deformation of metallic glasses can generally be described as homogeneous at high temperature and inhomogeneous at low temperatures.

The homogeneous plastic deformation of BMGs can be thought of as the viscous flow of an undercooled fluid and usually occurs at T >0.7 T_g. Steady-state flow tests suggest that homogeneous flow involves a balance between structural disordering and ordering (free volume creation and annihilation) [42]. Also the steady-state condition implies that the structural parameters are determined by external parameters such as temperature and stress, and hence remain constant during plastic flow. At room temperature, however, inhomogeneous plastic flow is the main plastic deformation mode and is characterized by the formation and propagation of shear bands until final fracture. The transition temperature from homogeneous flow to inhomogeneous flow can be compared with the ductile-to-brittle transition temperature in crystalline metals. Indeed, at high stresses and lower temperatures BMGs deform exclusively through localization in shear bands which is the reason for the name ‘inhomogeneous’ [41].

1.5.4 Plasticity and Fracture toughness

Plasticity describes the deformation of materials undergoing non-reversible changes of shape in response to applied stress. In metallic glasses, plasticity is accommodated through the formation of shear bands, accompanied by the creation of free volume during deformation. Interestingly, if BMGs show room-temperature plasticity, the stress–strain curve is serrated with repeated drops of ~1% in stress as indicated in Fig. 5 [47]. Unlike crystalline metals, the serration here might be related to the release of a shear band that then ceases to operate. Recently, a stress-driven process for explaining shear banding behavior was supposed by Ketov [48]. When stresses drop below a certain value and are not high enough to maintain plastic deformation, shear band propagation would stop and wait for a subsequent rise of stress.

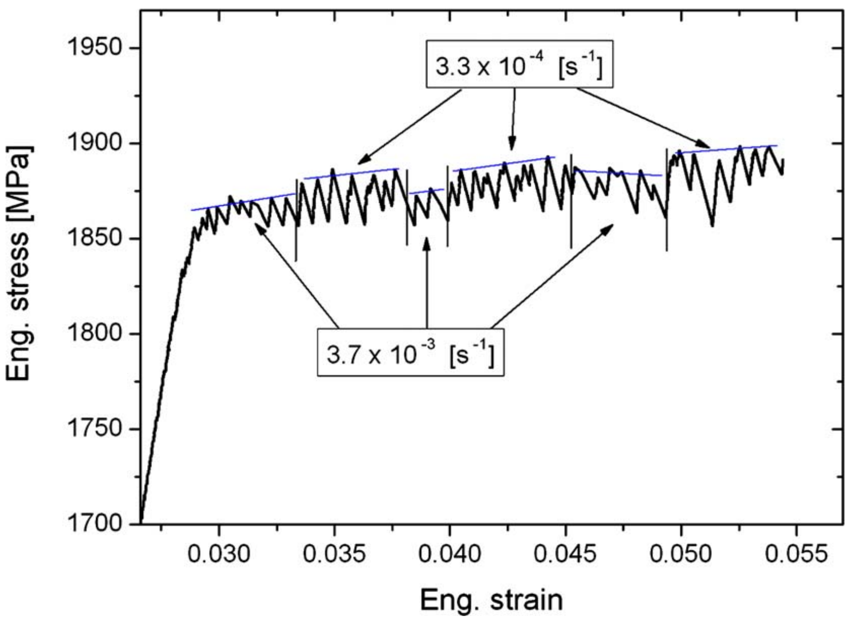

Figure 5. Compressive stress/strain curve of Vitreloy 105 at different strain rate. Reprinted with permission from [47].

Fracture toughness is an important indicator of damage tolerance for mechanical applications and is often used in material specification. In addition, toughness values are assumed to be intrinsic properties of BMGs. Because using elastic constants as an indicator to understand plasticity and fracture of metals is well accepted [49], the suggestion of a correlation between toughness and Poisson's ratio ν has been influential in designing BMGs with improved plasticity [50]. Recently the nature of the correlation was widely studied and it was found that a higher plasticity and/or toughness are correlated with a higher Poisson's ratio. Schroers and Johnson [51] proposed that the large compressive plasticity of a Pt-based BMGs is correlated to the high Poisson ratio of ν = 0.42, which allows for extending of shear bands rather than forming detrimental cracks. Deformation is therefore accomplished by the formation of multiple shear bands, which results in the observed large global ductility and high fracture toughness. Liu et al [33] also created BMGs that have relative large ν and the resulting BMGs can sustain extremely high deformation without fracture both in compression and in bending at room temperature. Recently, Madge et al.

[52] made an attempt to correlate the toughness of variety of glassy alloys and the findings suggest the toughness increases gradually with ν in mode II fracture. Therefore, the pursuit of higher values of ν remains worthwhile to achieve higher toughness BMGs. Since a finer shear band spacing, and consequently smaller shear offsets, will improve plasticity, it is reasonable to consider that the combination of Poisson's ratio and toughness property can be linked to the nature of shear banding. The analyses of Conner et al. [53] and of Wei et al. [54] both show that the shear-band spacing and the shear offset depend on ν: as ν approaches its upper bound of 0.5, the shear-band spacing can decrease to near zero.

Moreover, many studies have shown that the fracture toughness of ductile BMGs exhibits a high degree of specimen-to-specimen variability [55, 56]. Recently Narayan et al. [35] demonstrate that the observed high variability is a result of highly variable propensity for the conversion of shear bands into cracks which can be attributed to a high sensitivity to variability in the critical load, P_{cr}, at which cracks initiate at shear bands. Accordingly, it is reasonable to hypothesize that a heterogeneous structure that promotes a higher number of shear bands and block excessive shear band propagation can reduce the scatter.

The plastic flow always occurs in a small region which is called plastic or process zone at the tip of a sharp crack in a material. Plastic flow blunts the crack and thus, a lower yield stress, promoting plastic flow, tends to increase toughness. The process-zone size r_p can be described by an equation: $r_p=K_c^2/\pi\sigma_y^2$. For most BMGs, they usually have exceptionally high yield strength, so even those also with high fracture toughness values would have rather small process zones.

1.6 Application potential as structural materials

As noted in section 1.3, BMGs are susceptible to crystallization. To avoid this, rapid cooling is always required to form a glass and the cooling rate imposes a significant restriction on the casting thickness. Even though current research focusing on the optimization of compositions for high glass-forming ability makes good progress in expanding the critical casting thickness (from 1mm to >1cm), there is still a long way to go for BMGs to be applied as structural materials. In addition, as it is noted above that the process-zone sizes are small for most metallic glasses, thus the best applications for them would be in small components. Metallic glasses are, indeed, attractive for use in MEMS (microelectromechanical systems) devices. Their good elastic properties are prominent while their weak points like low plasticity are unimportant for small scale components. When sample size goes down to the nm regime to have a length-scale similar to that of shear bands which has length-scale of 10-20nm in thickness, the shear bands will contribute a more significant role in the sample. The sample size effects are also observed in metallic plates in bending: thin plates typically exhibit higher ductility and toughness while thicker plates of the same composition show brittle fracture behavior [53, 57]. Analogous to Griffith's theory, the critical stress for propagating a pre-existing shear band scales inversely with sample size. Therefore, small sample size suppresses shear band localization and homogeneous deformation throughout the sample dominates at a high stress level which is followed by necking fracture [58].

Though bulk metallic glasses have some useful functional properties, the current interests are mainly in the potential of their structural uses. Their unique properties make them attractive for many potential applications. At present MGs are more expensive than conventional alloys, mostly because one or some of the elementary components is expensive. In some cases, (e.g. Pd), the element is intrinsically expensive; in other cases, the cost is increased because the elements (e.g. Zr) have to be of particularly high purity (in the case of zirconium it is expensive, but necessary, to have very low oxygen content). Even if the raw material costs are not so high, the lack of established mass production methods restricts availability and raises prices. Another problem is that there are limited compositions for BMGs and most of them are patented with limited accessibility. Nonetheless, we can expect an ongoing reduction in the cost of BMG components as new compositions are developed that use inexpensive metals, and as improved processing methods permit the use of base metals of lower purity.

2. Methods for improving the ductility and toughness of metallic glasses

2.1 Brief introduction

Both hot- and cold-working can be used to optimize mechanical properties of conventional polycrystalline metals, and there is also such interest in exploring similar possibilities for metallic glasses. At high temperatures, metallic glasses exhibit viscous flow which does not produce changes in structure or properties. Attention has therefore been focused on the effects of cold-working. Masumoto and Maddin [59] reported that cold-rolling could reduce hardness, Young’s modulus, and fracture strength of Pd-Si amorphous alloys. Since then useful microstructural features like arrays of shear bands induced by cold deformation such as wire drawing and cold-rolling have been explored extensively. Subsequent work [60, 61] has mostly attributed plasticity by rolling to the development of an inhomogeneous microstructure with soft and hard regions. The soft regions are preferred locations for initial deformation on subsequent loading and may assist initiation of new shear bands. The hard regions inhibit catastrophic propagation of shear bands and force the branching and proliferation of shear bands. Inhomogeneity can be induced by mechanical treatments and this does also improve plasticity of BMGs. The common mechanical treatments mainly include uniaxial compression, shot-peening, cold-rolling, and some new methods such as rapid-defect printing and imprinting [15, 61-64]. To improve plasticity, developing metallic-glass based composites has also been favored recently and such composites have shown good ductility and toughness [16, 65]. From these recent results it is clear that both mechanical treatments of BMGs and design of BMG composites can promote plasticity and high toughness by achieving more fine and uniform shear band patterns.

It has been widely recognized that, in addition to the structural effects noted above, cold-working is likely to induce residual stresses, and that such stresses may have an influence on the property changes that result. In conventional engineering materials, compressive surface stresses have very beneficial effects, ranging from increased fracture strength in silicate glasses to increased fatigue resistance in polycrystalline metal alloys. For metallic glasses, compressive surface stresses can also be induced by some surface treatment methods such as shot-peening and imprinting.

2.2 Uniaxial compression

By studying BMG cylinders plastically deformed by compression along their axis, He et al. [62] explored the importance of shear-band orientation. The low-aspect-ratio cylinders were deformed to compressive strains as great as 46%. Cuboid samples were cut from the deformed cylinders and tested in compression in a direction parallel to a diameter of the original cylinder. In these compression tests, the as-cast Zr-based BMG showed a plastic strain of 1.1%. As a result of prior compression the strain increased to a maximum of 12.1% for compressive pre-strain of 29% on the original cylinder. On increasing compression of the original cylinders, straight primary shear-band traces appeared at ~45º to the loading axis, and wavy secondary traces appeared perpendicular to the axis. The population of primary shear bands increased with increasing compression, up to a maximum again at 29% imposed plastic strain. In contrast, the population of secondary shear bands continued to increase sharply. Noting that both the population of primary shear bands and the plasticity of the cuboids decreased for plastic strains exceeding 29% on the original cylinders, He et al. suggested that the plasticity of the cuboids cut from the compressed cylinders was directly proportional to the density of the primary shear bands, implying that plasticization effect of pre-induced shear bands depends on their orientation.

Related results were obtained by Yu et al. [66] on a wide variety of 2-mm-diameter BMG rods pre-loaded in compression parallel to the diameter prior to axial compressive testing. It was found that for intermediate levels of pre-loading, substantial increases in compressive plasticity could be achieved. For example, the failure strain of Vitreloy 105 can be increased from 1% in the as-cast glass to 10% in the glass when optimally pre-loaded.

2.3 Cold-rolling

As reported by Scudino et al. [61], the influence of cold-rolling (Fig. 6) on structure, thermal stability, and room temperature compressive and tensile mechanical properties of the Vitreloy 105 bulk metallic glass has been investigated. Cold-rolling does not affect the thermal stability of the glass. However, it induces the formation of several shear bands and creates a heterogeneous microstructure consisting of hard and soft regions, as demonstrated by hardness measurements. As a result of the generation of such structural heterogeneities, the room temperature plastic deformation of the metallic glass is significantly improved: the compressive plastic strain increases from 1.1% for the as-cast material to 2.6% for the cold-rolled sample. Also, the tensile ductility increases from 0% for the as-cast samples to 0.8% for the cold-rolled samples.

Similar results were also observed by Lee [60]. In their study the intrinsic plasticity of $Zr_{44}Ti_{11}Cu_{9.8}Ni_{10.2}Be_{25}$ and $Zr_{55}Ti_{5}Al_{10}Cu_{20}Ni_{10}$ bulk metallic glasses (BMGs) were improved from 0.5% up to 15% plastic strain due to the introduction of microstructural inhomogeneity upon cold rolling at room temperature. This approach shows an easy way to overcome the intrinsic brittleness of the BMGs by modifying their physical properties, which enables easy nucleation and branching of multiple shear bands upon unconstrained loading during the compression test.

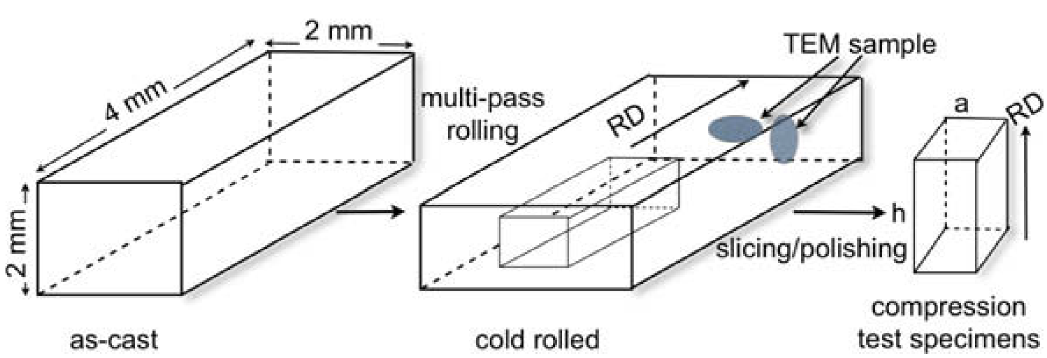

Figure 6. Schematic view of cold rolling of the as-cast samples. Reprinted with permission from [60].

2.4 Shot-peening

Y. Zhang et al. suggested in their work that the stress profile in an as-cast BMG cylinder is of the parabolic form: tensile stress in the center, compressive stress in the two sides [67]. They used a Zr-based BMG known as Vitreloy1 ($Zr_{41.2}Ti_{13.8}Cu_{12.5}Ni_{10}Be_{22.5}$) that is widely characterized. After the surfaces of the BMGs were shot-peened, surface roughness of 1.3μm was observed. A cross-section through the peened layer showed shear bands to a depth of 80μm. Indentation tests on the cross-section showed that the measured hardness decreases in the shear-banded surface layer, indicating a softening of 10%. The reason is attributed to plastic flow in metallic glasses localizing into shear bands associated with work softening. Micro-hardness tests were conducted on the roughened peened surfaces. An increase in the measured surface hardness was observed, but it cannot be attributed to work hardening. In both cases there are competing trends: softening by introduction of shear bands and hardening by residual stress. In the cross-section the softening is the predominant factor, while on the surface of peened layer the hardening (compressive residual stress) predominates. The biaxial compressive stress in the surface leads to a smaller plastic zone underneath the indenter, causing more pile-up and increased hardness. In another study, a fully amorphous BMG known as LM-001 ($Zr_{21.5}Ti_{42}Cu_{15.5}Ni_{14.5}Be_{3.5}Al_3$) was tested in the four-point flexural configuration by Raghavan et al [68]. The surfaces of as-cast BMGs were shot-peened with cast steel balls with 280 μm mean diameter. Nanoindentation technique was used to test the hardness of peened material and a higher hardness value of 9 GPa on peened surface compared to 7.6 GPa in the bulk was recorded which are similar results as observed in Zhang's study discussed above. Zhang et al. attributed this hardness difference to that the indent diameter was similar to the thickness of the peened layer and therefore the measured values are the combination effects of peened layer and bulk. However, different sample preparation process and indentation techniques (depth of penetration was less than one-tenth of peened layer) were used in Raghavan's study, the possibility that the combination of peened and bulk material contributing to increased hardness was ruled out. Therefore, the enhanced hardness is only attributed to biaxial residual stress present on the peened surface but not in the bulk. The even higher hardness in surface also indicates that compressive residual stresses completely negate the strain softening and make the plastic flow more difficult than in the bulk. The result that cross-section of the peened layer is considerably softer than that of the bulk is similar to Y. Zhang et al.

2.5 Rapid defect-printing

The principle for rapid defect printing (RDP) is illustrated schematically in Fig. 7 [64]. A thick plate with a design of distributed “defect makers” in the surface can be used as the printing mold, which is installed in a machine. The polished BMG sample is pressed using the printing molds with sharp “defect makers” by the machine, and defects can thus be rapidly printed onto the two surfaces of the sample.

Previous work has indicated that the method of introducing designed artificial defects as mechanical heterogeneities is effective in producing multiple shear bands and achieving macroscopic tensile plasticity in monolithic BMGs [69]. Principally, the effectiveness of the present method is closely related to the unique characteristics of BMGs derived from the shear banding deformation mechanism. Thus the method of designed artificial defects to improve plasticity may be applicable only for BMGs, but not for metallic crystalline materials. The proposed RDP treatment can introduce surface defects in a rapid, convenient and effective way, which facilitates its potential industrial application. The results from this study also indicate that, by simply doing some surface treatment to introduce geometrical and mechanical heterogeneities, the poor plasticity of monolithic BMGs with large critical size can be distinctly improved.

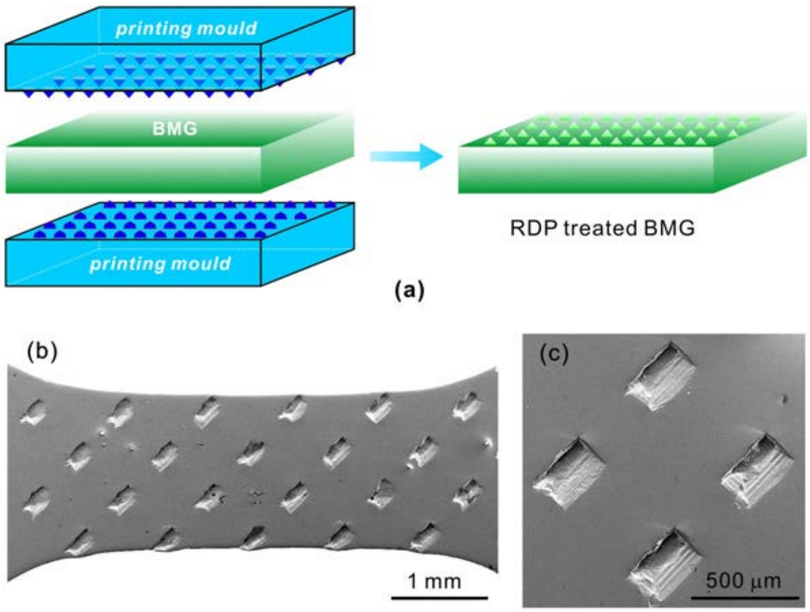

Figure 7. Illustration of process of RDP treatment. (a) Illustration of processes of RDP treatment; (b) BMG sample finally obtained for tension testing; (c) detailed observation of the introduced surface defects. Reprinted with permission from [64].

2.6 Imprinting

As shown by Scudino et al. [15], imprinting is another surface treatment that can improve the plasticity of BMGs. They pressed a parallel-ridged template into the surfaces of a tensile-test specimen cut from a Zr-based BMG plate at room temperature (Fig. 8). The imprinted troughs were parallel to the tensile axis. As shown in micro-hardness maps (Fig. 9) of the 2-mm-wide gauge length of the specimen, the imprinting leads to a marked inhomogeneity: softening under the imprints and hardening between them, associated with plastic flow and with, respectively, tensile and compressive residual stresses. Recently, spatially resolved strain maps (Fig. 10) have been created by high-energy X-ray diffraction [70]. Fig. 10(c) shows the strain components of the different atomic shells in the X-Y plane of the imprinted sample. The tangential pattern ε_{xx} displays a strong compressive strain field directly under the imprinted X-Z surface, which becomes tensile at Y ~ -0.2 mm. A similar behavior can be observed for the axial pattern ε_{yy}, where the magnitude of the strain is reduced with respect to the tangential ε_{xx} pattern. The shear pattern ε_{xy} related to r_1 mainly consists of strain field with positive values with a few isolated areas with negative values. The results confirmed that imprinting creates a spatially heterogeneous atomic arrangement consisting of strong compressive and tensile strain fields. The imprinting leads to more diffuse yielding, starting at lower stresses, and, importantly, distinctly improved ductility of up to 0.9% (compared to essentially zero ductility in the as-cast material). Scudino et al. attributed the improved ductility to the easy initiation of shear bands in the soft regions and the blocking of potentially catastrophic shear-band propagation by the hard regions.

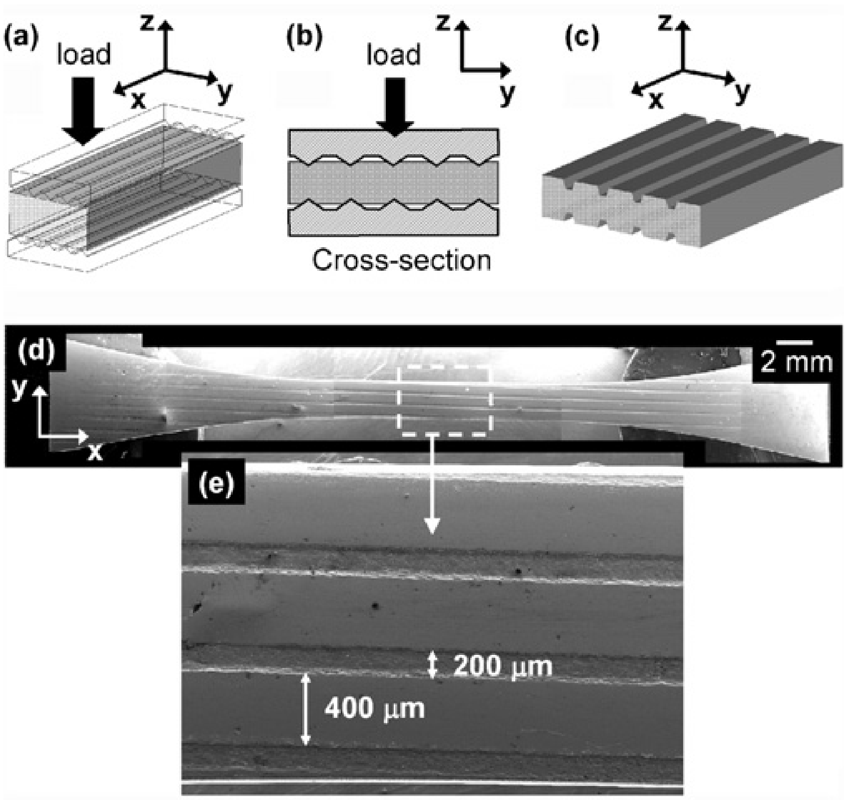

Figure 8. (a–c) Schematic representation of the imprinting process. (d–e) Resulting surface morphology after imprinting the $Zr_{52.5}Ti_5Cu_{18}Ni_{14.5}Al_{10}$. Reprinted with permission from [15].

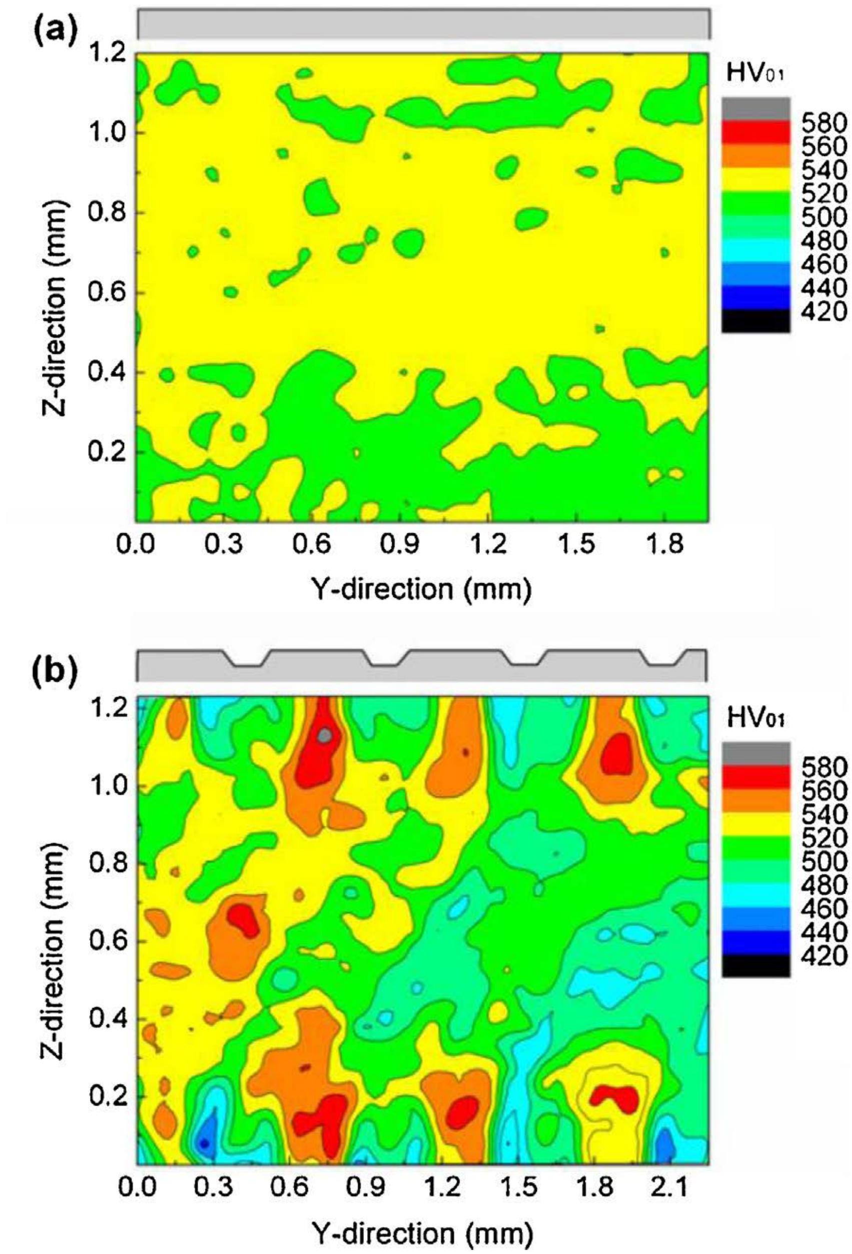

Figure 9. Hardness maps of (a) as-cast and (b) imprinted metallic glass reveal the creation of a heterogeneous microstructure consisting of alternating hard and soft regions. Reprinted with permission from [15].

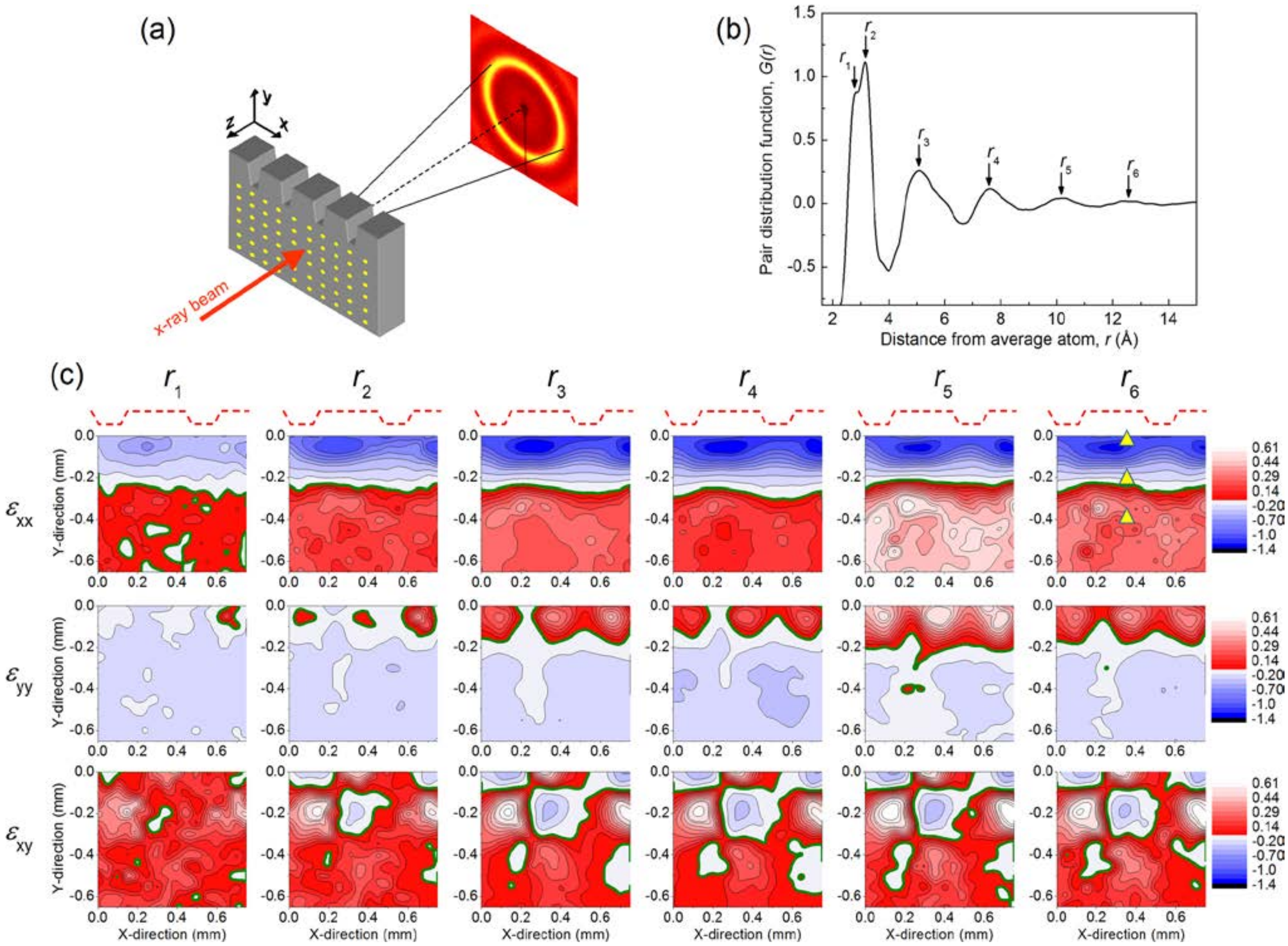

Figure 10. (a) Schematic illustration of the setup for the XRD measurements. The yellow spots represent the position where the diffraction patterns were taken. (b) Example of pair distribution function $G(r)$ showing the position of the peaks *ri* used to evaluate the strain generated in the plastically deformed BMG. (c) Strain maps of the e_{xx}, e_{yy}, and e_{xy} components evaluated from the different *ri* peaks. The dashed red lines indicate the position of the imprints.

2.7 BMG Composites

Besides improving mechanical behavior by cold deformation, designing metallic glass based composites has also attracted much interest. Hays et al. [16] studied the ductile metal reinforced Vitreloy 1 ($Zr_{41.2}Ti_{13.8}Cu_{12.5}Ni_{10}Be_{22.5}$) BMG matrix composites. By controlling cooling rate, partial crystallization and subsequent dendritic growth of β phase were obtained. The length-scale of dendrites lies in the range of 50 to 150 μm and radius of about 1.5-2 μm. The dendrite/matrix interface in this composite is sharp and strong by the fact that most interfaces remain intact during loading and yielding. Compared to Vitroley 1 that has a total yield strain of 2%, the composite shows a strain over 8% which demonstrated obvious strain hardening behavior contributed by the ductile phase. Also due to the embedded secondary phase, the yield strength drops from 1.9 GPa for BMGs to 1.7 GPa for the composites. Both of these two changes of mechanical properties indicate “the averaging behavior” brought by the ductile phase. That is because the embedded secondary particles can serve as heterogeneous sites for multiple shear bands initiation and can also block their propagation.

It is evident that by producing in situ secondary phase or adding ex situ particles [71], improved plasticity can be achieved by generating more uniform shear bands and blocking the activated ones. Further investigations should focus on the optimization of size of secondary phase and strength and stability of interface; however, such work is beyond the scope of this thesis.

3. Aim of the thesis

The aim of this project was to advance the understanding of fracture behavior of bulk metallic glasses by three-point bending tests and explore the results and mechanism of one kind of surface mechanical treatment on mechanical properties. Based on the fracture mechanics parameters and experimental observations, the correlation between fracture toughness and fracture morphology was developed.

Improving plasticity of BMGs can be achieved by controlling shear bands, such as shear band spacing, shear band propagation, etc. If more shear bands can be introduced and thus the pattern of shear bands is finer, plastic strain will distribute more evenly in each shear band. In addition, delaying the crack initiation at the activated ones can also provide positive effects. Introducing inhomogeneity to glassy microstructure has been suggested [15] to be effective for plasticity improvement and crack initiation delay. Therefore, surface mechanical treatment was deployed to give as-cast BMG samples inhomogeneity. One recently developed method involves loading BMG plates between two imprinting tools with a regular array of linear teeth which leads to a marked inhomogeneity with soft regions under the imprinted areas and hardening between them [15]. Such imprinting improves tensile plastic deformation to ~0.9%; however, to date no measurements of fracture toughness of imprinted samples have been reported. Therefore, the purpose of this project is to test the hypothesis that imprinting will improve the fracture behavior of a Zr-based BMG.

4. Experimental Procedures

The $Zr_{52.5}Ti_5Cu_{18}Ni_{14.5}Al_{10}$ (at.%) BMG was chosen for the present experiments. Commonly known as Vitreloy 105, this BMG has good glass-forming ability but relative low compressive plasticity (~0.8%) and often zero tensile ductility. Furthermore, the fracture toughness is reported to be highly scattered for as-cast sample, which presents a challenge for engineers to predictably and safely design components using this BMG.

An ingot with nominal composition $Zr_{52.5}Ti_5Cu_{18}Ni_{14.5}Al_{10}$ was prepared by arc melting in a titanium-gettered argon atmosphere. The ingot was remelted several times in order to achieve a homogeneous master alloy. From this ingot, a plate with dimension of 2 × 40 × 40 mm^3 was prepared by centrifugal casting. Imprinting was carried out at room temperature as schematically shown in Figs. 8(a-c). The glassy sample was placed between two imprinting hardened steel tools with a regular array of linear teeth. A load of 22 kN was then applied along the *z*-direction for 1 minute and, as a result, a periodic pattern of linear imprints is created on the *x*-*y* surface of the glass. The resulting width of imprinted regions was ~235 μm while the un-imprinted regions had a width of ~370 μm. After imprinting process, samples were carefully ground and polished to remove imprints and leave a flat sample surface.

The nominal dimensions of single edge notch bend, SEN(B), beams used for fracture toughness tests were thickness B =2 mm, width W =4 mm, length L =20 mm, as is shown in Fig. 11. All as-cast and imprinted samples were gradually ground and polished to 0.05 μm surface finish. A straight, through-thickness notch was made by diamond blade with a root radius of ~170 μm, followed by a micro-notch with a root radius of ~8 μm which was cut by sliding a razor blade across the notch with a 1 μm diamond paste. Fatigue pre-cracking was performed by cycling the sample with a 25 Hz sine wave with a ratio of minimum to maximum load of $R=P_{min}/P_{max} = 0.1$ using a computer controlled electro-mechanical test machine (ElectroForce 3200, Bose Corporation, Eden Prairie, MN, USA). To initiate pre-cracks, the required applied stress intensity range $\Delta K = K_{max} - K_{min}$, where K_{max} and K_{min} and are the maximum and minimum stress intensity applied to the sample during loading cycle, was consistently between 6 MPa √ m and 9

MPa $\sqrt{m}$ for the samples. After pre-cracking, the crack length, *a*, of each sample was between 0.46W and 0.68W as permitted by ASTM standard E1820 for J-integral based testing. Three-point bending fracture toughness tests were conducted using a 15.2 mm loading span on a computer controlled servo-hydraulic testing machine (Model 8501, Instron Corporation, Norwood, MA, USA) with a 5 kN load cell and a constant displacement rate of 0.83μm s^{-1}. Post fracture samples were observed by scanning electron microscopy (QUANTA 600F, FEI, Hillsboro, OR, USA).

Nanoindentaton experiments (NanoTest Vantage, Micro Materials, Wrexham, UK) were conducted on the sample side face to correlate fracture surface features with locally hard or soft regions. A Berkovich type indenter tip was used with a maximum load of 100 mN and a dwell period of 30 s at maximum load. Loading and unloading times were set as 20 s and 15 s, respectively, and the results of ten indents were averaged.

Finally, general line intercept procedures [72] were used to quantify the dimple sizes. For each sample, two representative dimple pattern microscopic photographs which have a magnification of ~1000× are selected for the measurement. A 14 x 14 grid lines with test line length of 140 mm was superimposed on each micrograph. The number of times each test line crossed the dimple pattern was counted and the dimple size was calculated using the length of line divided by the average number of intercepts. It should be noted that the dimple pattern measured by intercept method might be underestimated due to the fact that the lines might not cross the center of each dimple pattern.

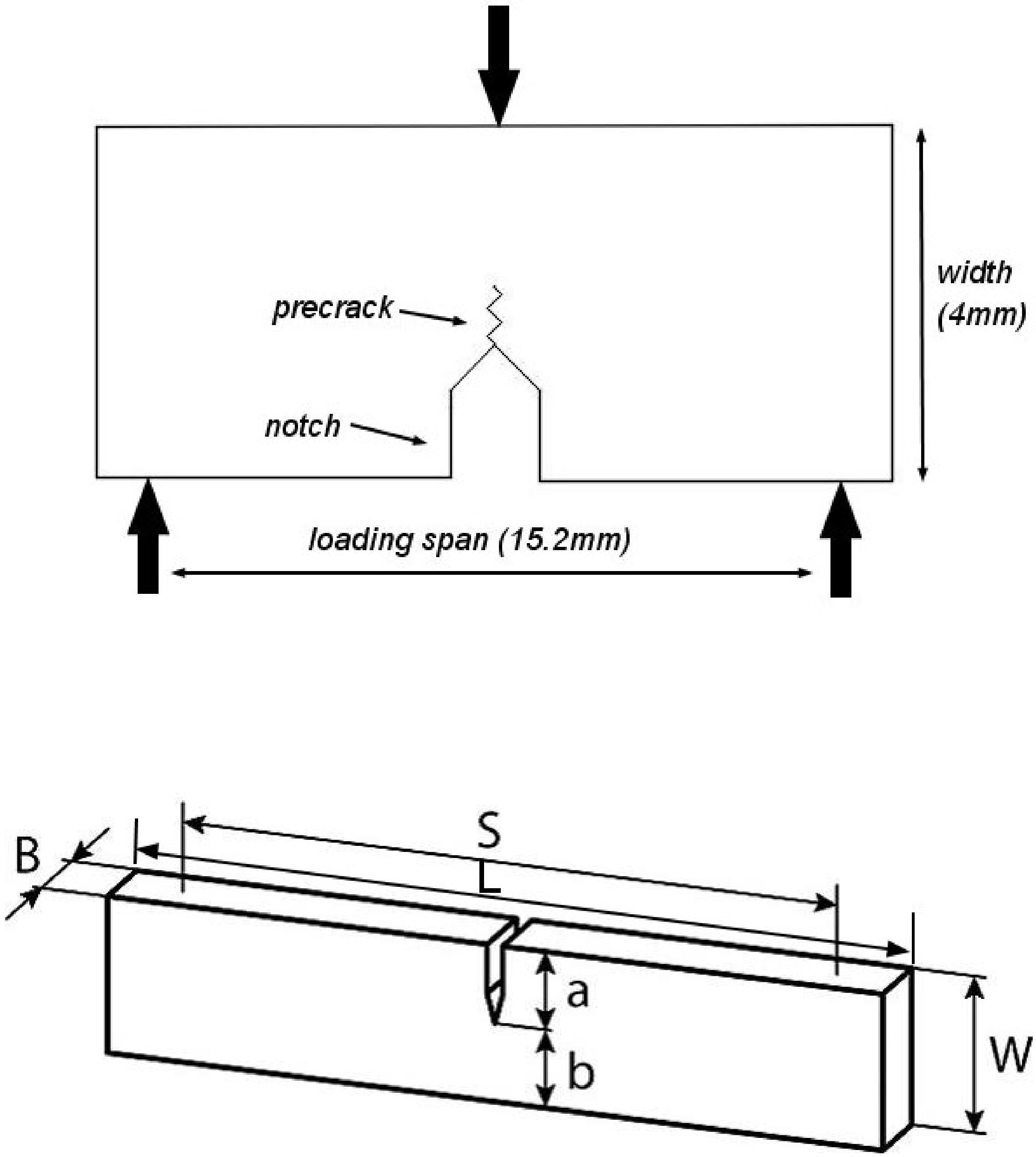

Figure 11. Schematic description of single edge notch specimen dimension.

5. Fracture mechanics and fracture toughness of Zr-based BMGs (results)

During a fracture toughness test, the deformation behavior of a metallic material can be described as linear-elastic, non-linear elastic, or elastic-plastic. In general, the different deformation behavior determines which fracture parameters should be used to characterize the values of fracture toughness. Therefore, two typical methods for measuring fracture toughness have been defined by ASTM standard. The first one is developed to determine the point value of plane strain fracture toughness K_{IC} or K-based fracture testing as described in ASTM standard E399 [73]. For the elastic-plastic deformation behavior, plastic deformation dominates ahead of crack tip, and thus J-integral or J-based fracture testing is always used to described fracture toughness which is defined in ASTM standard E1820 [74].

In both cases, conditional load P_Q should be calculated. Fig. 12 shows three different types of load-displacement curves for calculating P_Q. A 5% secant method is applied to determine P_Q in each load-displacement curve. In this 5% secant method, the 5% secant line with slope equal to 95% of the initial slope of the tangent OA to the initial linear portion of the record is constructed to determine P_5. In type I case, the force at every point on the record before P_5 is lower than P_5, then P_Q=P_5. For type II case, a small amount of crack initiates before P_5 and continues beyond the 5% secant line, P_Q is equal to the value where initiation begins. When fracture occurs before achieving 5% nonlinearity which is type III case, then P_Q=P_{max}. From the P_Q value obtained from load-displacement curve, conditional fracture toughness K_Q value is calculated from Eq. (4):

$$K_Q = \frac{P_Q S}{BW^{3/2}} f(\frac{a}{W}) \tag{4}$$

where for bend specimen f(a/W) is calculated from equation (5):

$$f\left(\frac{a}{W}\right)=3\sqrt{\frac{a}{W}}\cdot\frac{1.99-\left(\frac{a}{W}\right)\left(1-\frac{a}{W}\right)\left[2.15-3.93\frac{a}{W}+2.7\left(\frac{a}{W}\right)^{2}\right]}{2\left(1+2\frac{a}{W}\right)\left(1-\frac{a}{W}\right)^{3/2}} \tag{5}$$

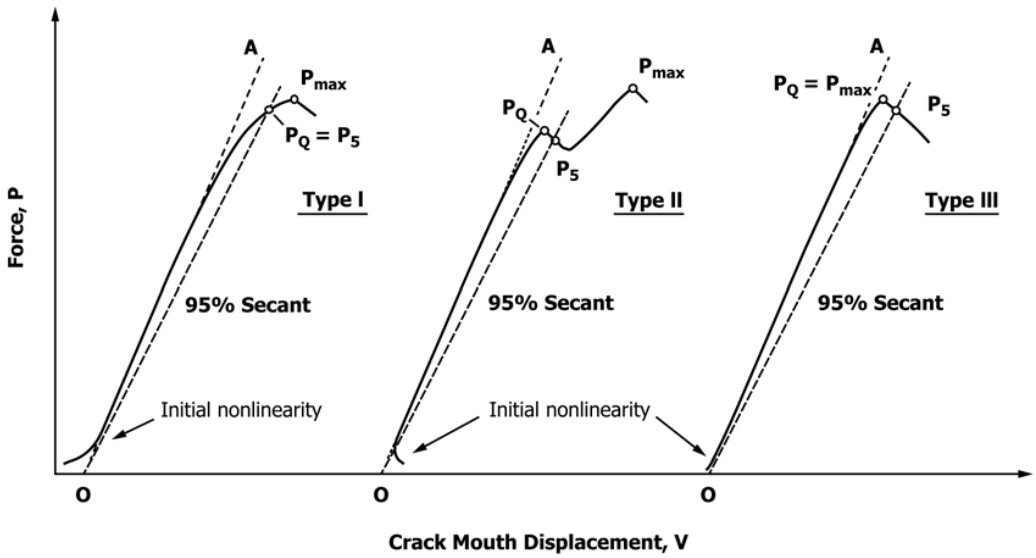

Figure 12. Three typical types of load-displacement curve.

To apply linear elastic fracture toughness testing as defined in ASTM E399, the initial allowed crack size a_0 is required to lie between 0.45W and 0.55W. In addition to the initial crack size requirement, another two validity requirements must also be met so that the conditional toughness K_Q is equal to K_{IC} and thus the fracture toughness test is considered as a valid test:

$$W-a\geq 2.5\left(\frac{K_Q}{\sigma_{ys}}\right)^2 \tag{6}$$

$$P_{max}\leq 1.1P_Q \tag{7}$$

For BMGs, as has been observed in previous studies [56], the toughness of as-cast Vitroley 105 BMG samples was scattered and tests did not consistently meet the requirement of valid K_{IC} fracture toughness testing. According, instead of K_{IC}, both K_Q values and K_J values are calculated based on the *J*-integral using Eq. (8) [1]

$$K_J = \sqrt{\frac{E(J_{el}+J_{pl})}{1-\nu^2}} \quad . \tag{8}$$

In Eq. (8), J_{el} and J_{pl} are the elastic and plastic components of the J-integral that can be calculated from Eq. (9) and Eq. (10), respectively:

$$J_{el} = \frac{K^2(1-\nu^2)}{E} \tag{9}$$

$$J_{pl} = \frac{\eta_{pl} A_{pl}}{Bb} \tag{10}$$

where η_{pl} = 1.9, A_{pl} is the area under force versus displacement curve, $b = W{-}a$, E and ν are Young's modulus and Poisson's ratio, respectively. The Young's modulus and Poisson's ratio were taken to be 85.6 GPa and 0.375, respectively [75]. As was found by Gludovatz et al. [56], it is assumed all results here are sample size dependent and specific to our chosen sample dimensions. The measured load-displacement curves were either linear to fracture (type III according to ASTM E1820) or showed plasticity before fracture (type I according to ASTM E1820). Examples of both curve types are shown in Fig. 13, and a summary of all results is shown in Table 2.

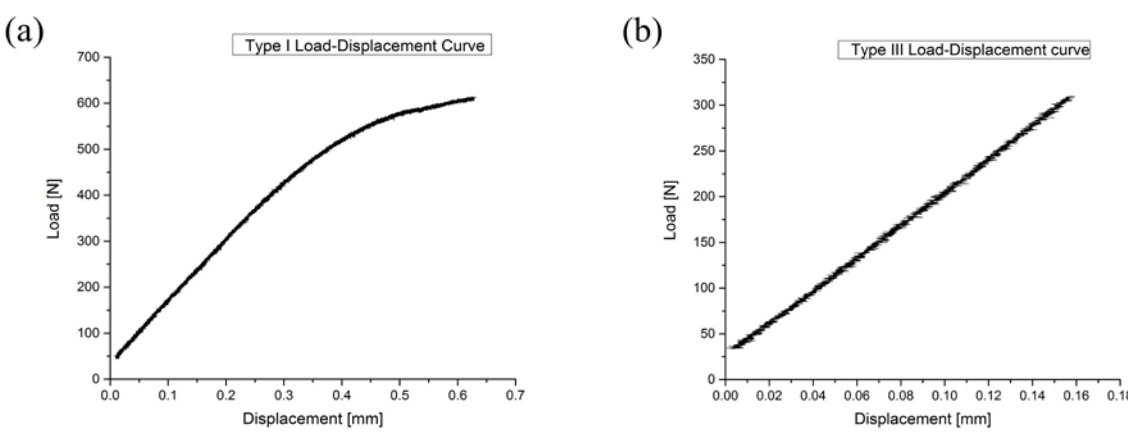

Figure 13. (a) Example type I Load/displacement curve for Sample Imprinted-3. (b) Example type III load/displacement curve for Sample As-cast-4.

Sample	a/W	L/D curve type	J_{el} (kJ/m^2)	J_{pl} (kJ/m^2)	J (kJ/m^2)	K_J (MPa√m)	K_Q (MPa√m)
Imprinted-1	0.58	Type I	32	107	139	118	41
Imprinted-2	0.60	Type I	52	60	112	106	56
Imprinted-3	0.64	Type I	102	20	122	110	88
Imprinted-4	0.56	Type I	196	41	237	154	118
Imprinted-5	0.68	Type I	58	8	66	81	73
Imprinted-6	0.66	Type I	85	86	171	131	70
Average					**141**	**116**	**74**
STDV					**58**	**24**	**27**
As-cast-1	0.57	Type I	131	165	296	171	91
As-cast-2	0.62	Type I	111	46	157	125	89
As-cast-3	0.46	Type I	78	33	111	105	76
As-cast-4	0.50	Type III	7	0	7	27	27
As-cast-5	0.59	Type III	11	0	11	33	33
As-cast-6	0.58	Type III	27	0	27	52	52
Average					**102**	**86**	**61**
STDV					**113**	**58**	**28**

Table 1. Summary of the fracture toughness results.

6. Designed heterogeneities improve the fracture reliability of a Zr-based bulk metallic glass (discussion)

Compared to as-cast samples, all imprinted samples showed obvious plasticity (type I) before fracture and less scattered toughness values in terms of J and K_J. For the as-cast samples, although half of them also deformed with some plasticity (type I), the other half failed with pure linear-elastic behavior (type III) leading to widely scattered K_J values that lie between 27 and 171 MPa √ m. Although the average toughness of the imprinted samples appears somewhat higher (K_J of 116 vs. 86 MPa√m), a student's t-test revealed this difference in average fracture toughness is not statistically significant. More importantly, all imprinted samples showed pronounced plastic behavior ($J_{pl}>0$) and the standard deviation was reduced dramatically from 58 to 24 MPa√m. Thus, it is concluded that imprinting toughens the more brittle as-cast samples while perhaps lowering the toughness of the toughest ones. Overall, imprinting is shown to reduce scatter and achieve a more consistent damage tolerant behavior with measurable plasticity.

Besides the improved fracture reliability reflected from J-integral and K_J values, imprinted samples also showed more tortuous crack trajectory than as-cast samples (Fig. 14). By matching the imprinting pattern wavelength to the crack path (white arrow) in Fig. 14a, it seemed that heterogeneities induced by imprinting process also have a positive effect on macroscopic crack propagation behavior.

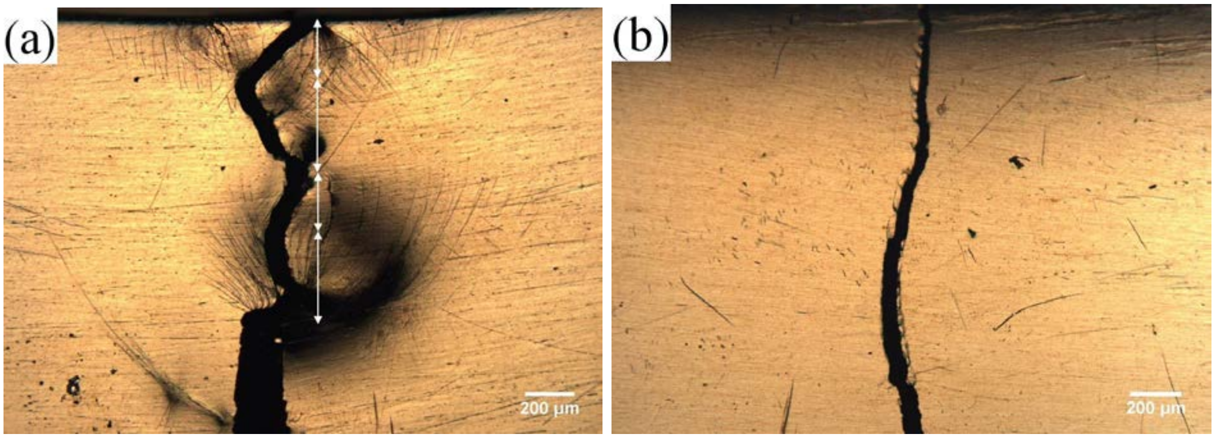

Figure 14. (a) Example crack trajectory of an imprinted sample (K_J=118 MPa√m) where the arrows match imprinting pattern wavelength. (b) Example crack trajectory of a low toughness as-cast sample (K_J=27 MPa√m). Cracks propagated from bottom to top.

As it is discussed by Scudino et al. [15], the imprinting process (Fig. 8) results in softer regions under imprints and harder regions between them. Furthermore, they attributed the hardness variations in part to the imprinting process creating tensile (under imprints) and compressive (between imprints) residual stress fields. This has been recently confirmed by high-energy x-ray diffraction studies showing the existence of a spatially heterogeneous atomic arrangement consisting of strong compressive and tensile strain fields [70]. In addition to the role of residual stresses, the imprinting process is expected to cause local strain-induced softening because of increased free volume. Consequently, the microstructure of imprinted samples can be considered as a network of strain-induced softened regions superimposed on a regular arrangement of compressive and tensile residual stresses. The easy initiation of shear bands in soft regions, and impeded propagation of activated ones by hard regions, is thought to contribute to the enhanced plasticity of imprinted samples. Accordingly, evidence of enhanced plasticity should be visible on the fracture surfaces.

The fracture surface of the type I samples (where $J_{pl} > 0$) showed four distinct regions on the fracture surface originating from the end of fatigue pre-crack (Fig. 15). Region I is a rather smooth region which is formed by crack blunting with multiple shear bands, shear sliding behavior can be seen in this area at high magnification. This region extends roughly 8 µm to 20 μm from the pre-crack for different samples with an average value of ~12 μm. After the crack blunting region, there is a transition to a typical vein pattern (region II) similar to that generated by tensile failures [76, 77]. Tandaiya et al. [78] refer to this region as the Taylor meniscus instability zone. These two regions (Fig. 15a) indicate where shear band sliding and subsequent fracture initiated. Region III and IV (Fig. 15b) contain dimple patterns similar to those commonly observed on BMGs fracture surfaces [14, 40]. Furthermore, region III is notably rougher than region IV and contains many stair-like ridges that run parallel to the crack propagation direction. As the fracture progressed, theses ridges disappear leaving a planar and generally flat fracture surface in Region IV with a uniform dimple pattern. The as-cast samples with relative high fracture toughness and ductile type I load-displacement behavior had fracture surfaces that were generally similar to the imprinted ones. In contrast, for the low toughness type III as-cast samples (where $J_{pl} = 0$), region I extended only ~4 μm from the pre-crack and there is no evidence of region III.

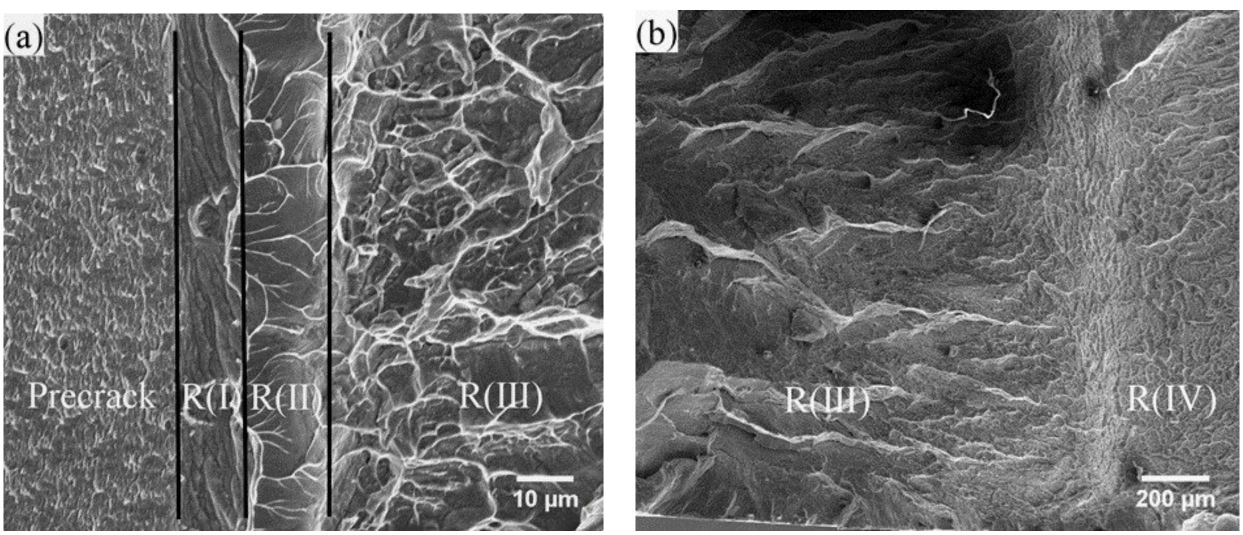

Figure 15. (a) An example of regions I and II and the beginning of Region III seen on the fracture surfaces of type I samples. (b) Last two regions of fracture surfaces in type I samples. Crack propagated from left to right.

In the narrow region at the onset of region I, the observed average shear band spacing of imprinted samples is ~13μm, whereas the shear band spacing averaged ~41μm for the as-cast samples. The lower shear bands spacing for the imprinted material indicates a higher shear band density formed in this area during crack blunting. According to Schuh et al. [43], the percolation of shear transformation zones (STZs) promotes the formation and propagation of shear bands. Scudino et al [15] have attributed the improved ductility of the imprinted samples to the ease of initiating shear bands in the soft regions since these higher free volume and tensile residual stress areas give a lower potential energy barrier for STZ operation. Therefore, the STZs are more easily activated and shear bands are more easily initiated than in the hard regions.

Narayan et al. have recently suggested the large scatter in mode I fracture toughness for BMGs can be attributed to the mode I toughness being highly sensitive to variability in the critical load, P_{cr}, at which cracks initiate at shear bands [79]. Accordingly, it is reasonable to hypothesize that a heterogeneous structure that promotes a higher number of shear bands, and thus more homogenously distributes the load across many shear bands, can reduce the scatter. Furthermore, a high shear band density should give rise to a more homogeneous distribution of plastic strain, more crack blunting, and higher toughness. Since the crack tip opening displacement should be linearly proportional to the J-integral, Fig. 16 shows the J-integral at fracture plotted against the measured average crack blunting zone size for each sample. A trend of increasing J-integral with increasing crack blunting zone size is seen in Fig. 16. A linear regression gives a p-value of 0.0052 which indicates the trend is statistically significant.

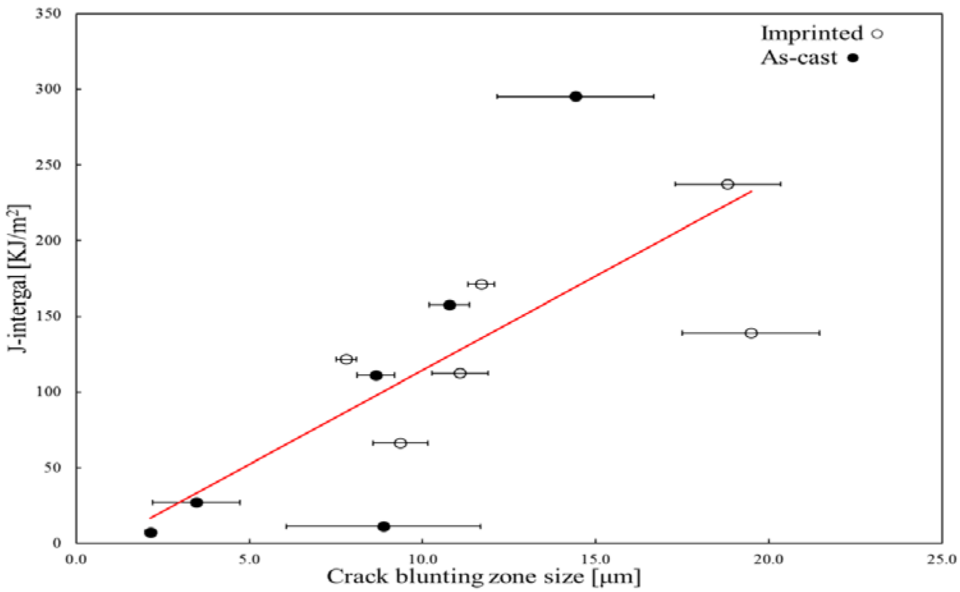

Figure 16. Correlation of the *J*-integral at fracture with crack blunting zone size of both imprinted and as-cast material.

In region II, the river-like vein pattern extending to a length-scale of ~16µm between regions I and III can be observed. The formation of a vein pattern may be associated with a high fluidity originating from softening caused by profuse shear bands initiation from region I [80]. Since this fracture surface feature indicates low inner material viscosity [81], it is correlated to the beginning of unstable sliding of shear bands.

Regions III and IV generally consist of dimple patterns, although some areas of more vein like patterns were seen in the imprinted samples. Often larger dimples contain several smaller ones (Fig. 17), suggesting a process of small microvoids coalescing to form larger ones. Fig. 17c shows the dimple size is significantly smaller for the brittle, low toughness samples. In contrast, the size difference between the imprinted and high toughness as-cast samples is not significant (Fig. 17a and 17b). The line intercept measurements revealed that the dimples sizes of imprinted samples range from 7 to 12µm, whereas 1 to 9µm for as-cast samples (Table 3). Fig. 18 shows that there is linear relationship between dimple size *w* and $(K_J/\sigma_y)^2$ of BMG Vitreloy 105. Clearly, *w* increases with the increase of $(K_J/\sigma_y)^2$. Based on imprinted and as-cast yield strength values, a correlation between the K_J toughness value and dimple pattern sizes is constructed as: w=0.0014 $(K_J/\sigma_y)^2$, where w is the length scale of dimple size and σ_y is the yield strength. The coefficient of the linear fit in this equation is about ten times smaller than that of Xi et al., who reported a linear correlation between the length scale of the dimple pattern and the fracture toughness w=0.025 $(K_{IC}/\sigma_y)^2$ [82]. That difference might be caused by underestimating the dimple sizes with the line intercept method. However, it is not clear what method was used to quantify the dimple size in the Xi et al. study. In their study, a range of BMG compositions found to exhibit the characteristic dimple pattern at different length scales ranging from ~20 nm in brittle Fe-based metallic glass ($Fe_{46}Ni_{32}V_2Si_{14}B_6$) to the ~60 μm tough Zr-based BMG ($Zr_{41}Ti_{14}Cu_{12.5}Ni_{10}Be_{22.5}$). It should be noted that the BMG material ($Zr_{52.5}Ti_5Cu_{18}Ni_{14.5}Al_{10}$) in this project which has an average dimple size ~10 μm was not included in the Xi et al. study. Therefore, the difference of the coefficient could be related to the different measurement method and/or the different composition of the BMGs selected.

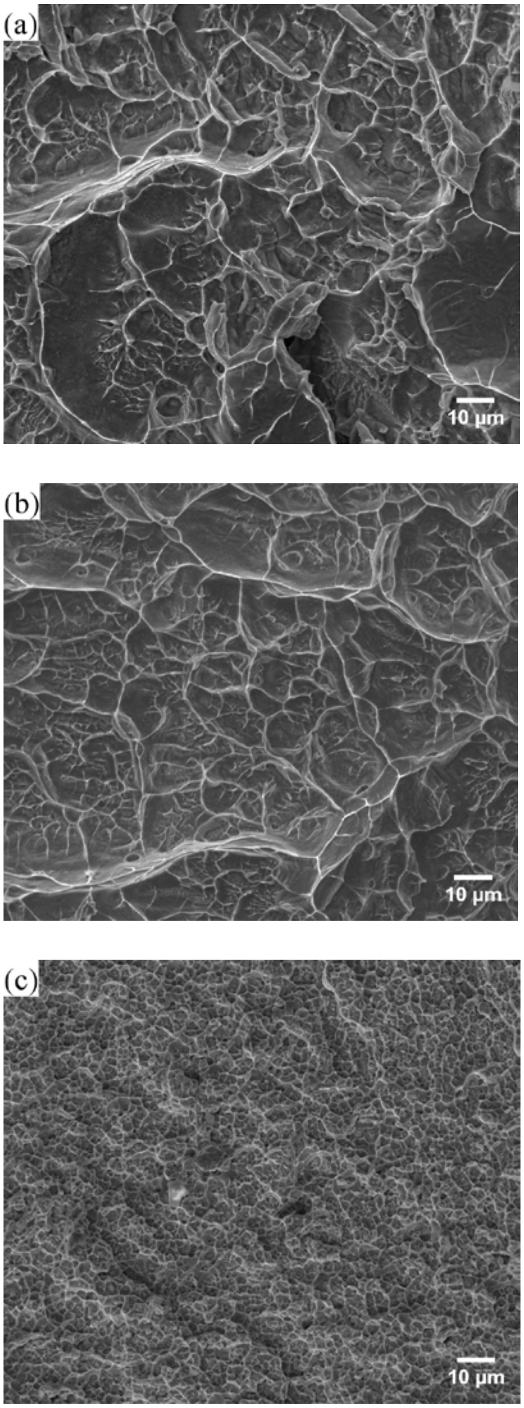

Figure 17. (a) Dimple pattern of an imprinted sample in Region IV (K_J = 110 MPa√m). (b) Dimple patterns of an as-cast sample with high toughness (Type I) in Region IV (K_J = 125 MPa√m). (c) Dimple pattern of an as-cast sample with relatively low toughness (Type III) in Region IV (K_J = 27 MPa√m). Cracks propagated from left to right.

Sample #	K_J (MPa√m)	Dimple size (μm)
Imprinted-1	118	8.6
Imprinted-2	106	7.6
Imprinted-3	110	9.3
Imprinted-4	154	12.5
Imprinted-5	81	6.9
Imprinted-6	131	10.1
Average	**116**	**9.2**
STDV	**24**	**2.0**
As-cast-1	171	9.6
As-cast-2	125	8.3
As-cast-3	105	5.6
As-cast-4	27	1.7
As-cast-5	33	2.9
As-cast-6	52	3.8
Average	**86**	**5.3**
STDV	**58**	**3.1**

Table 2. Results of measurement of dimple sizes by line intercept method.

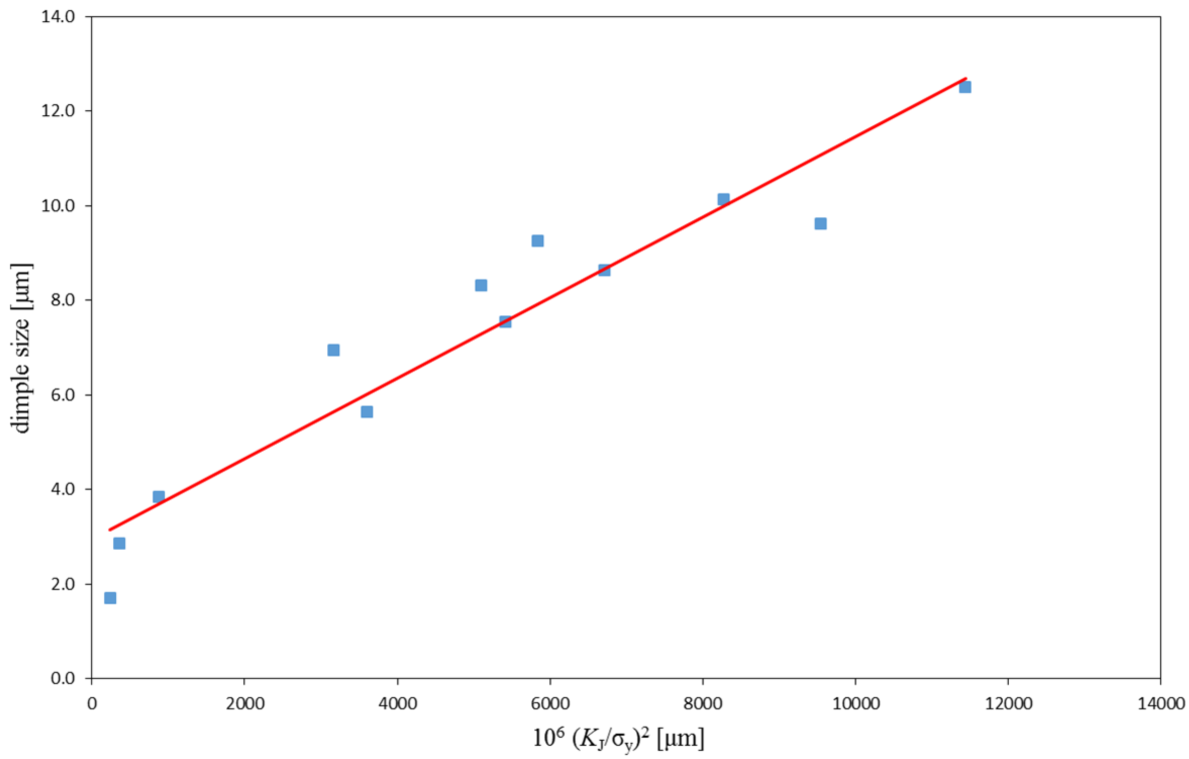

Figure 18. Correlation of fracture toughness to dimple size.

As mentioned above, region III is seen only in the imprinted and high toughness as-cast samples and is associated with crack bifurcation (Fig. 19a). Fig. 19b shows a magnified view of a large step that runs along the crack growth direction for the imprinted sample with the highest toughness (K_J=154 MPa √ m). The crack bifurcation leads to mode III tearing between the bifurcated cracks giving high toughness and leaving stair-like steps on the fracture surface. The steps show a typical vein pattern caused by extensive shear sliding occurring during the crack opening fracture process, as was also observed in [80]. Similar crack bifurcation behavior was also seen in the high toughness type I as-cast samples (Fig. 19c), but not in the more brittle type III as-cast samples (Fig. 19d) in which a very flat fracture surface is seen after the Taylor meniscus instability zone. This suggests the complex stress state caused by crack bifurcation and mode III tearing between the bifurcated cracks contributes to high fracture toughness, and imprinting to create a heterogeneous structure promoted this toughening mechanism in all samples. In contrast, for as-cast samples this toughening mechanism only occurs in some samples that presumably evolved sufficient structural heterogeneity during casting. Accordingly, the fracture toughness for the as-cast samples is much more highly scattered.

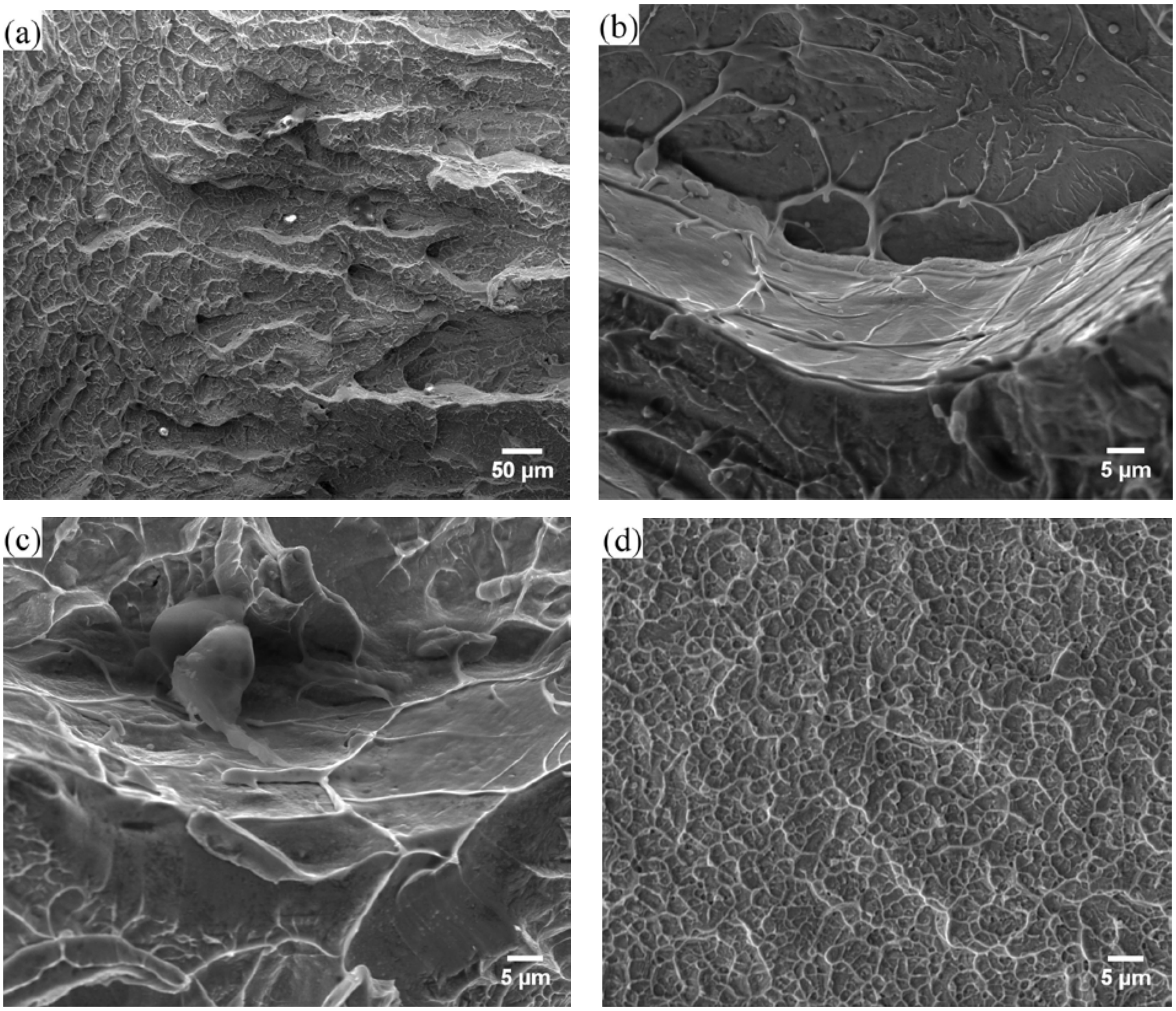

Figure 19. (a) An overview of the beginning of crack bifurcation (K_J=154 MPa√m). (b) Shear step in an imprinted sample (K_J=154 MPa√m). (c) Shear step in a ductile type I as-cast sample (K_J=171 MPa√m). (d) No apparent crack bifurcation or shear sliding in brittle type III as-cast samples (K_J = 33 MPa√m). Crack propagated from left to right.

Finally, by correlating regions of high and low shear bands density observed on the sample sides to the fracture surfaces, it is observed that there are also corresponding changes on the fracture surface from a dimpled pattern to a more river like vein pattern, as shown in Figs. 20a and 20b. The band seen in the center of Fig. 20a is ~220 μm wide, which correlates well to the ~200 μm soft regions under the imprints (Fig. 8e). Nanoindentation results on the side face also indicate that the more river-like vein pattern corresponds to the relatively soft area under an imprint with an average hardness value of 6.6±0.2 GPa on the sample side, whereas the dimple pattern corresponds to the area between imprints with an average hardness value of 7.2±0.2 GPa. A student's *t*-test showed this hardness difference to be statistically significant (p-value≪0.05). In these soft regions a more river-like vein pattern is observed (Fig. 20b) which as mentioned above suggests the fluidity of the BMG was higher in these regions. The pattern change is also associated with shear bands being deflected by the hard regions which act as obstacles to shear bands propagation.

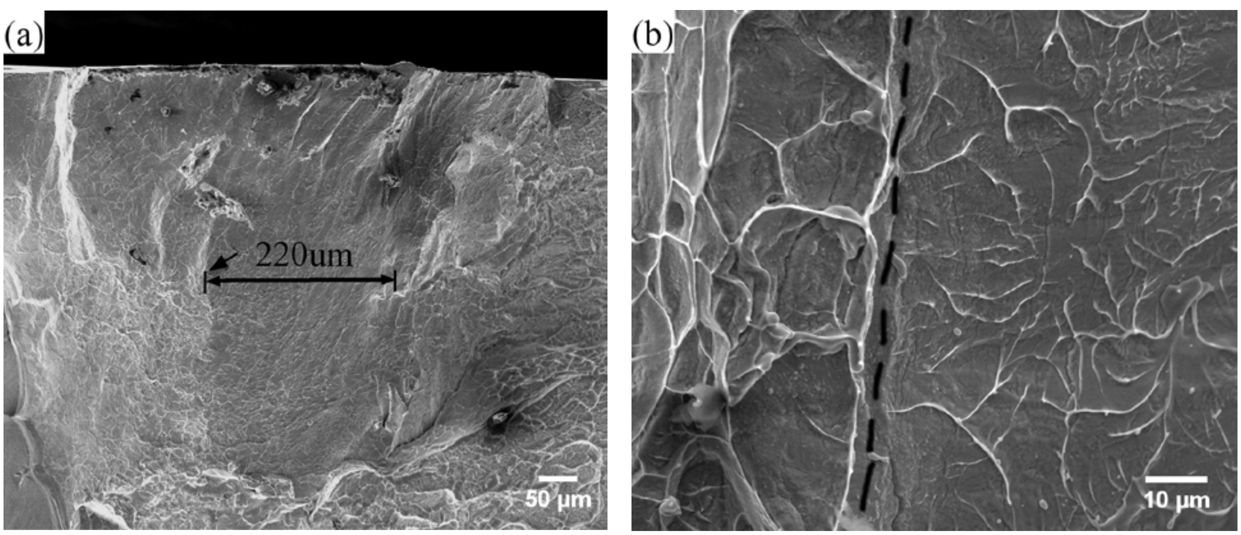

Figure 20. (a) Pattern changes on the fracture surface of an imprinted sample in local Region III and Region IV. (b) Magnified view of the pattern change at the location marked by black arrow in 7(a). Crack propagated from left to right.

7. Summary and Conclusions

In conclusion, the present results indicate that mechanical imprinting of BMGs to produce a heterogeneous structure of hard and soft regions is effective at ductilizing BMGs and reducing the scatter in mode I fracture toughness. Although the increase in mean fracture toughness was not statistically significant in this study, it is clear that imprinting improved the ductility and toughness of the most brittle as-cast samples. Indeed, all imprinted samples showed a plastic contribution to *J*-integral while only 50% of the as-cast samples showed any plasticity. Macroscopically, the imprinting process promoted a tortuous crack path with crack bifurcation that contributed to the toughness. The ability to create BMGs with consistent damage tolerance properties is important to the future success of BMGs for many mechanical applications. Overall, while this study demonstrates imprinting can ductilize BMGs and reduce scatter in the mode I toughness, it is also important to recognize this is an initial study and the mechanical treatment parameters (imprint dimensions, imprinting force, imprinting pattern, etc.) have not been optimized. With further optimization, there is an expectation that imprinting, or similar mechanical treatments, can definitively increase the average toughness as well.

References:

[1] A. Hirata, L.J. Kang, T. Fujita, B. Klumov, K. Matsue, M. Kotani, A.R. Yavari, M.W. Chen, Science, 341 (2013) 376-379.
[2] C. Suryanarayana, A. Inoue, Bulk metallic glasses, CRC Press, Boca Raton, FL, 2011.
[3] S. Gravier, G. Kapelski, M. Suery, J.J. Blandin, Int J Appl Glass Sci, 3 (2012) 180-187.
[4] D. Turnbull, Contemporary physics, 10 (1969) 473-488.
[5] J.F. Loffler, J. Schroers, W.L. Johnson, Appl Phys Lett, 77 (2000) 681-683.
[6] W. Klement, R. Willens, P. Duwez, Nature, 187 (1960) 869-870.
[7] C.A. Pampillo, H.S. Chen, Mater Sci Eng, 13 (1974) 181-188.
[8] A. Peker, W.L. Johnson, Appl Phys Lett, 63 (1993) 2342-2344.
[9] X.H. Lin, W.L. Johnson, J Appl Phys, 78 (1995) 6514-6519.
[10] A. Inoue, T. Zhang, T. Masumoto, Mater T Jim, 31 (1990) 425-428.
[11] A. Inoue, T. Nakamura, N. Nishiyama, T. Masumoto, Mater T Jim, 33 (1992) 937-945.
[12] A. Inoue, N. Nishiyama, T. Matsuda, Mater T Jim, 37 (1996) 181-184.
[13] C.J. Gilbert, R.O. Ritchie, W.L. Johnson, Appl Phys Lett, 71 (1997) 476-478.
[14] P. Lowhaphandu, J.J. Lewandowski, Scripta Mater, 38 (1998) 1811-1817.
[15] S. Scudino, B. Jerliu, S. Pauly, K.B. Surreddi, U. Kuhn, J. Eckert, Scripta Mater, 65 (2011) 815-818.
[16] C.C. Hays, C.P. Kim, W.L. Johnson, Phys Rev Lett, 84 (2000) 2901-2904.
[17] H. Choi-Yim, R. Busch, U. Koster, W.L. Johnson, Acta Mater, 47 (1999) 2455-2462.
[18] X.H. Lin, W.L. Johnson, W.K. Rhim, Mater T Jim, 38 (1997) 473-477.
[19] J.M. Barandiaran, J. Colmenero, J Non-Cryst Solids, 46 (1981) 277-287.
[20] H. Men, D.H. Kim, J Mater Res, 18 (2003) 1502-1504.
[21] Y. Li, S.J. Poon, G.J. Shiflet, J. Xu, D.H. Kim, J.F. Loffler, Mrs Bull, 32 (2007) 624-628.
[22] A. Inoue, Sci Rep Res Tohoku A, 42 (1996) 1-11.
[23] D.B. Miracle, Nat Mater, 3 (2004) 697-702.
[24] H.W. Sheng, W.K. Luo, F.M. Alamgir, J.M. Bai, E. Ma, Nature, 439 (2006) 419-425.
[25] C.P. Chuang, P.K. Liaw, J.J. Kai, W. Dmowski, J.H. Huang, G.P. Yu, Adv Eng Mater, 15 (2013) 287-294.
[26] J. Wen, Y.Q. Cheng, J.Q. Wang, E. Ma, J Appl Phys, 105 (2009).
[27] Z.P. Lu, C.T. Liu, J Mater Res, 19 (2004) 427-428.
[28] D.R. Nelson, Defects and geometry in condensed matter physics, Cambridge University Press, Cambridge ; New York, 2002.
[29] D.R. Nelson, Phys Rev Lett, 50 (1983) 982-985.
[30] A. Di Cicco, A. Trapananti, S. Faggioni, A. Filipponi, Phys Rev Lett, 91 (2003).
[31] D.R. Nelson, Phys Rev B, 28 (1983) 5515-5535.
[32] J. Ding, S. Patinet, M.L. Falk, Y.Q. Cheng, E. Ma, P Natl Acad Sci USA, 111 (2014) 14052-14056.
[33] Y.H. Liu, G. Wang, R.J. Wang, D.Q. Zhao, M.X. Pan, W.H. Wang, Science, 315 (2007) 1385-1388.
[34] M.F. Ashby, A.L. Greer, Scripta Mater, 54 (2006) 321-326.
[35] K.K. Cameron, R.H. Dauskardt, Scripta Mater, 54 (2006) 349-353.
[36] J.J. Kruzic, Metall Mater Trans A, 42A (2011) 1516-1523.
[37] C.P. Chuang, T. Yuan, W. Dmowski, G.Y. Wang, M. Freels, P.K. Liaw, R. Li, T. Zhang, Sci Rep-Uk, 3 (2013).
[38] M.L. Morrison, R.A. Buchanan, P.K. Liaw, B.A. Green, G.Y. Wang, C. Liu, J.A. Horton, Mat Sci Eng a-Struct, 467 (2007) 190-197.

[39] S.E. Naleway, R.B. Greene, B. Gludovatz, N.K.N. Dave, R.O. Ritchie, J.J. Kruzic, Metall Mater Trans A, 44A (2013) 5688-5693.
[40] C.J. Gilbert, V. Schroeder, R.O. Ritchie, Metall Mater Trans A, 30 (1999) 1739-1753.
[41] A.S. Argon, Acta Metall Mater, 27 (1979) 47-58.
[42] C.A. Schuh, T.C. Hufnagel, U. Ramamurty, Acta Mater, 55 (2007) 4067-4109.
[43] C.A. Schuh, A.C. Lund, Nat Mater, 2 (2003) 449-452.
[44] F. Spaepen, Acta Metall Mater, 25 (1977) 407-415.
[45] J. Eckert, J. Das, S. Pauly, C. Duhamel, J Mater Res, 22 (2007) 285-301.
[46] B.P. Kanungo, S.C. Glade, P. Asoka-Kumar, K.M. Flores, Intermetallics, 12 (2004) 1073-1080.
[47] F.H. Dalla Torre, A. Dubach, M.E. Siegrist, J.F. Loffler, Appl Phys Lett, 89 (2006).
[48] S.V. Ketov, D.V. Louzguine-Luzgin, Sci Rep-Uk, 3 (2013).
[49] S.F.Pugh, Philosophical Magazine, 45 (1954) 823-843.
[50] J.J. Lewandowski, W.H. Wang, A.L. Greer, Phil Mag Lett, 85 (2005) 77-87.
[51] J. Schroers, W.L. Johnson, Phys Rev Lett, 93 (2004).
[52] S.V. Madge, D.V. Louzguine-Luzgin, J.J. Lewandowski, A.L. Greer, Acta Mater, 60 (2012) 4800-4809.
[53] R.D. Conner, W.L. Johnson, N.E. Paton, W.D. Nix, J Appl Phys, 94 (2003) 904-911.
[54] Y.J. Wei, X.Q. Lei, L.S. Huo, W.H. Wang, A.L. Greer, Mat Sci Eng a-Struct, 560 (2013) 510-517.
[55] A. Kawashima, H. Kurishita, H. Kimura, T. Zhang, A. Inoue, Mater Trans, 46 (2005) 1725-1732.
[56] B. Gludovatz, S.E. Naleway, R.O. Ritchie, J.J. Kruzic, Acta Mater, 70 (2014) 198-207.
[57] R.D. Conner, Y. Li, W.D. Nix, W.L. Johnson, Acta Mater, 52 (2004) 2429-2434.
[58] H. Guo, P.F. Yan, Y.B. Wang, J. Tan, Z.F. Zhang, M.L. Sui, E. Ma, Nat Mater, 6 (2007) 735-739.
[59] T. Masumoto, R. Maddin, Mater Sci Eng, 19 (1975) 1-24.
[60] M.H. Lee, K.S. Lee, J. Das, J. Thomas, U. Kuhn, J. Eckert, Scripta Mater, 62 (2010) 678-681.
[61] S. Scudino, B. Jerliu, K.B. Surreddi, U. Kuhn, J. Eckert, J Alloy Compd, 509 (2011) S128-S130.
[62] L. He, M.B. Zhong, Z.H. Han, Q. Zhao, F. Jiang, J. Sun, Mat Sci Eng a-Struct, 496 (2008) 285-290.
[63] Y. Zhang, W.H. Wang, A.L. Greer, Nat Mater, 5 (2006) 857-860.
[64] R.T. Qu, Q.S. Zhang, Z.F. Zhang, Scripta Mater, 68 (2013) 845-848.
[65] D.C. Hofmann, J.Y. Suh, A. Wiest, G. Duan, M.L. Lind, M.D. Demetriou, W.L. Johnson, Nature, 451 (2008) 1085-U1083.
[66] H.B. Yu, J. Hu, X.X. Xia, B.A. Sun, X.X. Li, W.H. Wang, H.Y. Bai, Scripta Mater, 61 (2009) 640-643.
[67] Y. Zhang, W.H. Wang, A.L. Greer, Nat Mater, 5 (2006) 857-860.
[68] R. Raghavan, R. Ayer, H.W. Jin, C.N. Marzinsky, U. Ramamurty, Scripta Mater, 59 (2008) 167-170.
[69] R.T. Qu, J.X. Zhao, M. Stoica, J. Eckert, Z.F. Zhang, Mat Sci Eng a-Struct, 534 (2012) 365-373.
[70] S. Scudino, H.S. Shahabi, M. Stoica, I. Kaban, B. Escher, U. Kuhn, G.B.M. Vaughan, J. Eckert, Appl Phys Lett, 106 (2015).
[71] J.M. Park, J.H. Han, N. Mattern, D.H. Kim, J. Eckert, Metall Mater Trans A, 43A (2012) 2598-2603.
[72] Standard Test Methods for Determining Average Grain Size, ASTM International, West Conshohocken, PA, 2013.
[73] A. Standard, E399-12e3,'Standard Test Method for Linear-Elastic Plane-Strain Fracture Toughness KIc of Metallic Materials', ASTM International, West Conshohocken, PA, 2012.
[74] A. standard, E1820-13e1,'Standard test method for measurement of fracture toughness', ASTM International, West Conshohocken, PA, 2013.
[75] J.H. Schneibel, J.A. Horton, P.R. Munroe, Metall Mater Trans A, 32 (2001) 2819-2825.
[76] Z.F. Zhang, J. Eckert, L. Schultz, Metall Mater Trans A, 2004, pp. 3489-3498.
[77] F. Spaepen, D. Turnbull, Scripta Metallurgica, 8 (1974) 563-568.
[78] P. Tandaiya, R. Narasimhan, U. Ramamurty, Acta Mater., 61 (2013) 1558-1570.

[79] R.L. Narayan, P. Tandaiya, G. Garett, M.D. Demetriou, U. Ramamurty, Scr. Mater., (2015) in press.
[80] J.Y. Suh, R.D. Conner, C.P. Kim, M.D. Demetriou, W.L. Johnson, J Mater Res, 25 (2010) 982-990.
[81] L.A. Deibler, J.J. Lewandowski, Mater. Sci. Eng. A-Struct. Mater. Prop. Microstruct. Process., 538 (2012) 259-264.
[82] X.K. Xi, D.Q. Zhao, M.X. Pan, W.H. Wang, Y. Wu, J.J. Lewandowski, Phys. Rev. Lett., 94 (2005p).